Cell

Transgenerational inheritance of acquired epigenetic signatures at CpG islands in mice

Graphical abstract

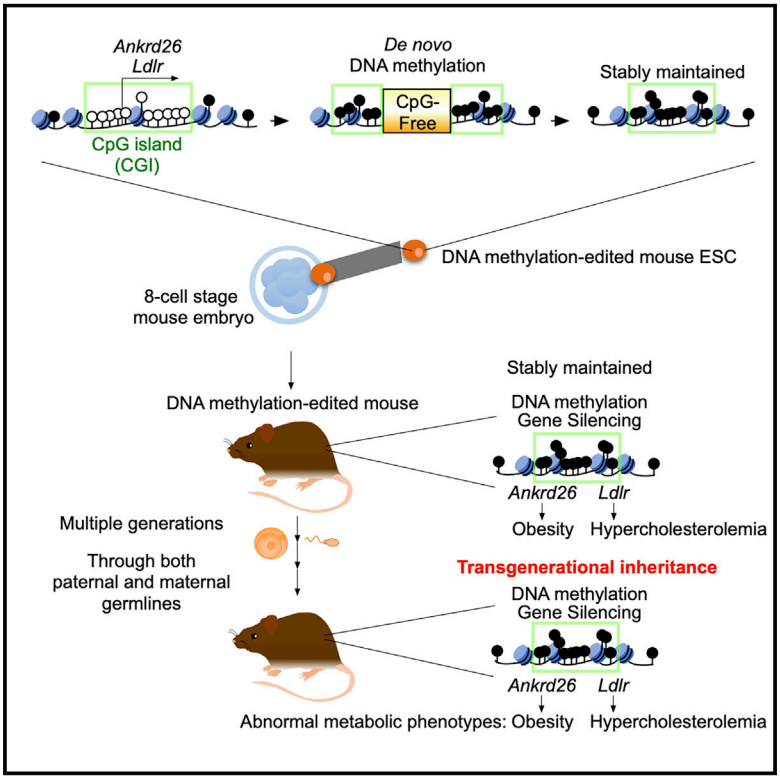

Highlights

- Establishment of targeted CGI methylation editing in mouse ES cells
- DNA methylation-edited mice exhibit phenotypic alterations induced by gene silencing
- Both acquired methylation and phenotypes are transmitted across multiple generations
- Heritable epigenetic memory reestablishes CGI methylation at the epiblast stage

Authors

Yuta Takahashi,
Mariana Morales Valencia, Yang Yu, ...,
Estrella Nuñez-Delicado,
Concepcion Rodriguez Esteban,
Juan Carlos Izpisua Belmonte

Correspondence

jcbelmonte@altoslabs.com

In brief

Takahashi et al. demonstrate that engineered epigenetic modifications and associated phenotypes can be transmitted across multiple generations in mammals.

Takahashi et al., 2023, Cell *186*, 715–731
February 16, 2023
https://doi.org/10.1016/j.cell.2022.12.047

Cell

CellPress

Article

Transgenerational inheritance of acquired epigenetic signatures at CpG islands in mice

Yuta Takahashi,[1,2] Mariana Morales Valencia,[1,2] Yang Yu,[1,3,4] Yasuo Ouchi,[1,2,5] Kazuki Takahashi,[1,2] Maxim Nikolaievich Shokhirev,[6] Kathryn Lande,[6] April E. Williams,[6] Chiara Fresia,[1] Masakazu Kurita,[1,7] Tomoaki Hishida,[1,8] Kensaku Shojima,[1] Fumiyuki Hatanaka,[1,2] Estrella Nuñez-Delicado,[9] Concepcion Rodriguez Esteban,[1,2] and Juan Carlos Izpisua Belmonte[1,2,10,*]

[1]Gene Expression Laboratory, Salk Institute for Biological Studies, 10010 North Torrey Pines Road, La Jolla, CA 92037, USA
[2]Altos Labs, 5510 Morehouse Drive, Suite 300, San Diego, CA 92121, USA
[3]Beijing Key Laboratory of Reproductive Endocrinology and Assisted Reproductive Technology and Key Laboratory of Assisted Reproduction, Ministry of Education, Center for Reproductive Medicine, Department of Obstetrics and Gynecology, Peking University Third Hospital, Beijing 100191, China
[4]Stem Cell Research Center, Peking University Third Hospital, Beijing 100191, China
[5]Department of Regenerative Medicine, Chiba University Graduate School of Medicine, 1-8-1 Inohana, Chuou-ku, Chiba 260-8670, Japan
[6]Integrative Genomics and Bioinformatics Core, Salk Institute for Biological Studies, 10010 North Torrey Pines Road, La Jolla, CA 92037, USA
[7]Department of Plastic, Reconstructive and Aesthetic Surgery, The University of Tokyo Hospital, Tokyo, Japan
[8]Laboratory of Biological Chemistry, School of Pharmaceutical Sciences, Wakayama Medical University, 25-1 Shitibancho, Wakayama, Wakayama, Japan
[9]Universidad Católica San Antonio de Murcia (UCAM), Campus de los Jerónimos, no. 135 Guadalupe 30107, Murcia, Spain
[10]Lead contact
*Correspondence: jcbelmonte@altoslabs.com
https://doi.org/10.1016/j.cell.2022.12.047

SUMMARY

Transgenerational epigenetic inheritance in mammals remains a debated subject. Here, we demonstrate that DNA methylation of promoter-associated CpG islands (CGIs) can be transmitted from parents to their offspring in mice. We generated DNA methylation-edited mouse embryonic stem cells (ESCs), in which CGIs of two metabolism-related genes, the Ankyrin repeat domain 26 and the low-density lipoprotein receptor, were specifically methylated and silenced. DNA methylation-edited mice generated by microinjection of the methylated ESCs exhibited abnormal metabolic phenotypes. Acquired methylation of the targeted CGI and the phenotypic traits were maintained and transmitted across multiple generations. The heritable CGI methylation was subjected to reprogramming in parental PGCs and subsequently reestablished in the next generation at post-implantation stages. These observations provide a concrete step toward demonstrating transgenerational epigenetic inheritance in mammals, which may have implications in our understanding of evolutionary biology as well as the etiology, diagnosis, and prevention of non-genetically inherited human diseases.

INTRODUCTION

Although it is largely accepted that biological inheritance is mainly driven by the inheritance of genomic DNA, epigenetic inheritance has been extensively documented in bacteria, protists, fungi, plants, and certain invertebrate animals,[1–11] further supporting the idea that, across evolution, there is more to heredity than simply inheritance of genomic DNA. In mammals, it is generally assumed that two distinct phases of epigenetic reprogramming serve to prevent inheritance of ancestral epigenetic signatures.[12–17] A genome-wide erasure of DNA methylation (as well as exchange of histone variants, and reduction of histone modifications) occurs in the primordial germ cells (PGCs), the gamete precursors.[18–23] This first reprogramming of the epigenome is followed by the reestablishment of epigenetic signatures and transcription profiles that enable gamete maturation and eventually fertilization. Global DNA methylation is once again erased post-fertilization in early pre-implantation embryos. Finally, as cellular differentiation ensues in post-implantation embryos, another round of global *de novo* methylation takes place.[24–26] This epigenome reprogramming may be incomplete, as certain regions, which are predominantly repeat associated, can escape full reprogramming of the PGCs epigenome.[19,22,23] These observations, together with reports suggesting the conveying of information to the offspring via epigenetic pathways,[1–8,10,27,28] may indicate the existence of mechanisms facilitating the transfer and/or reestablishment of ancestral epigenetic signatures to offspring in mammals. Although progress has been made recently, altogether, our knowledge of the extent and mechanisms by which parental epigenetic information in mammals is erased during this bimodal

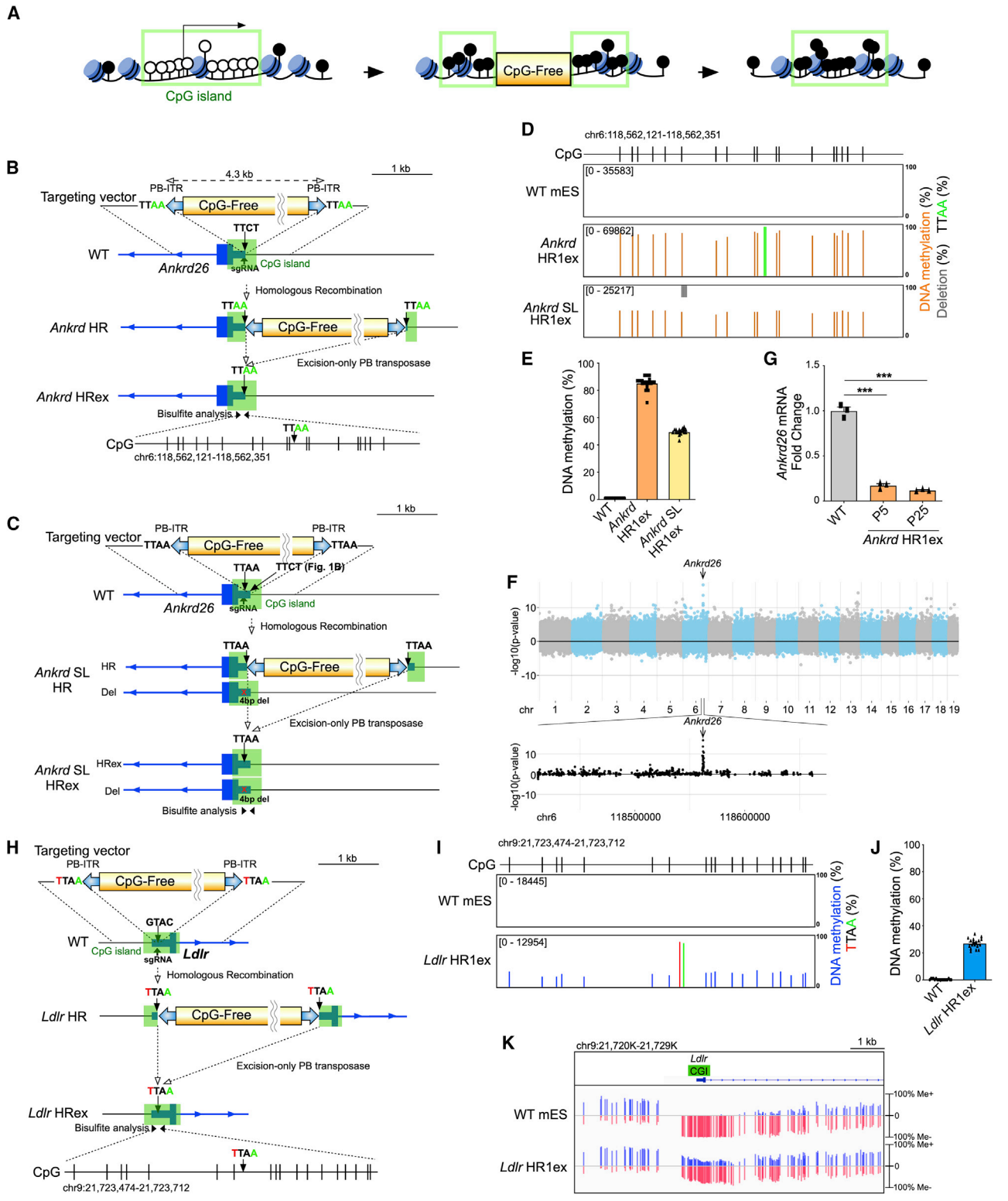

Figure 1. Generation of DNA methylation-edited mouse ESCs

(A–C and H) Schematics of targeted CpG island DNA methylation editing in mESCs.

(A) Integration of CpG-free DNA into CGI induces *de novo* DNA methylation of the entire targeted CGI and the methylation is stably maintained after the cassette removal. See also Figures S1 and S2.

(legend continued on next page)

and dynamic epigenetic reprogramming is still incomplete, and whether transfer of parental epigenetic marks can affect specific traits in their offspring, as well as its physiological relevance, remains debatable.

Cytosine-phosphate-guanine (CpG) islands (CGIs) are largely unmethylated regions with high frequencies of CpG that exist within the highly methylated mammalian genome, usually associated with promoter regions and subsequent initiation of gene expression. More than half of gene promoters are associated with CGIs.[29] Although CGIs-associated promoters predominantly remain unmethylated during development and life, epigenetic modifications, such as DNA methylation, of CGI regions can lead to gene silencing. Epimutations, such as abnormal CGI methylation, correlate with physiological alterations and diseases, including developmental defects, neural and metabolic disorders, and cancer.[30–34] Interestingly, some of these epimutations may be transmitted from parents to their offspring.[35–37] For example, epimutation of the DNA mismatch repair gene *MLH1*, a possible cause of non-polyposis colorectal cancer, was found in a mother who developed a colorectal cancer as well as her two children who also developed early colonic tumors, supporting transgenerational inheritance of CGI methylation.[36] However, these findings cannot exclude the possibility that these epimutations are secondary to *cis*-acting genetic variants and inherited genetic variants result in epimutations in their offspring. These and other observations prevent us from confidently concluding that CGI methylation is transmitted across generations through the parental germ line. Among the obstacles preventing this field from further advancement is the lack of DNA methylation-edited animal models, where targeted CGIs can specifically be *de novo* methylated in identical genetic backgrounds by targeted DNA methylation editing technologies.

Toward this end, we have developed a methodology that allowed us to demonstrate *in vitro* that integration of CpG-free DNA into CGIs could induce *de novo* DNA methylation of the entire targeted CGIs by disrupting the methylation-blocking machinery in human pluripotent stem cells (PSCs).[38] The *de novo* methylation was stably maintained even after CpG-free DNA removal, extensive passaging and cell differentiation.

Using this technology and to better ascertain whether transgenerational inheritance of CGI methylation may occur *in vivo* in mammals, we have generated DNA methylation-edited mice in which the targeted CGI of two different loci are methylated. The edited DNA methylation and ensuing phenotypes observed in the first-generation mice are maintained in subsequent generations, providing experimental evidence that epigenetic information, DNA methylation of CGIs, could be transmitted from parents to their offspring in mammals. Moreover, we have uncovered that the heritable DNA methylation of CGIs undergoes epigenetic reprogramming in PGCs and is subsequently reestablished in post-implantation embryos, providing initial insights into the mechanism underlying transgenerational inheritance of CGI methylation.

RESULTS

Targeted CGI methylation in mouse ESCs

The incidence of complex metabolic diseases has experienced a marked increase in the last two decades. Notwithstanding the well-known role of genetics in an organism's metabolism, inherited epigenetic metabolic disorders have also been proven in invertebrate model organisms and suggested in mammals.[8,39–46] For this study, as target loci, we selected two CGIs associated with metabolism-related gene promoters, the Ankyrin repeat domain 26 (*Ankrd26*) and low-density lipoprotein receptor (*Ldlr*). These genes were of particular interest, as knockout of *Ankrd26* or *Ldlr* results in obesity or hypercholesterolemia, respectively, but does not affect mouse viability and fertility.[47,48] Moreover, these target CGIs harbor the active status markers, histone H3K4me3 and H3K27ac, which we targeted in our previously established approach, in which integration of CpG-free DNA can induce stable *de novo* DNA methylation of the entire targeted CGIs (Figure 1A).[38] We constructed the targeting vectors such that they harbored homology arms on both sides of the CpG-free DNA; consisting of a promoter and neomycin resistant gene that were modified to remove all CpG sequences sandwiched by PiggyBac inverted terminal repeats (ITRs) (Figures 1B, 1H, S1A, and S2A) and then transfected to mouse embryonic stem cells (mESCs) with a plasmid expressing Cas9 nuclease and a single guide RNA (sgRNA). Expanding from our previous technology with human PSCs,[38] we targeted regions located near transcription start sites within the CGIs to ensure that the targeted CGIs acquire *de novo* DNA methylation by integration of CpG-free DNA in mESCs. Homologous recombination (HR) clones, in which the CpG-free cassette was properly integrated into the targeted CGIs on both alleles, were obtained after selection with G418 (Figures S1B, S1D, S2B, and S2D). For *Ankrd26* CGI targeting, four of eight HR clones exhibited *de novo* DNA methylation, of which two exhibited more than 55% of CpGs methylated (Figure S1C), indicating that integration of CpG-free DNA induced partial methylation of *Ankrd26* CGI for some HR clones. For *Ldlr* CGI targeting, two of nine HR clones exhibited *de novo* methylation and of those clones, ~35% of CpGs within the CGI were methylated (Figure S2C). These data show that integration of CpG-free DNA sporadically induces *de novo* DNA methylation of targeted CGIs in mESCs. When we introduced the CpG-free cassette into CGIs in hPSCs in our previous work, we observed that all targeted CGIs in HR clones exhibited *de novo* methylation with almost full methylation status.[38] This could be explained by differences in whole-genome *de novo* DNA methylation activity between mouse naive and human primed PSCs.[49,50]

(D, E, I, and J) Bisulfite sequencing analysis. (D and I) Each bar represents the methylation status of a single CpG site or percentage of TTAA or deletion allele. Number of mapped reads is shown in the columns. (E and J) Data represent mean ± SEM of methylation status of the 18 CpG sites in the CGIs.

(F) A Manhattan plot of differentially methylated regions between WT mESC and *Ankrd* HR1ex from WGBS. See also Table S1.

(G) Quantitative RT-PCR analysis of *Ankrd26* mRNA expression. Error bars indicate ±SEM of three independent experiments. Versus WT; ***$p < 0.0001$ by unpaired Student's t test.

(K) Target enrichment-genome bisulfite sequencing. Each vertical bar represents methylation status at a single CpG. Me+ and Me− represent methylated and unmethylated status, respectively.

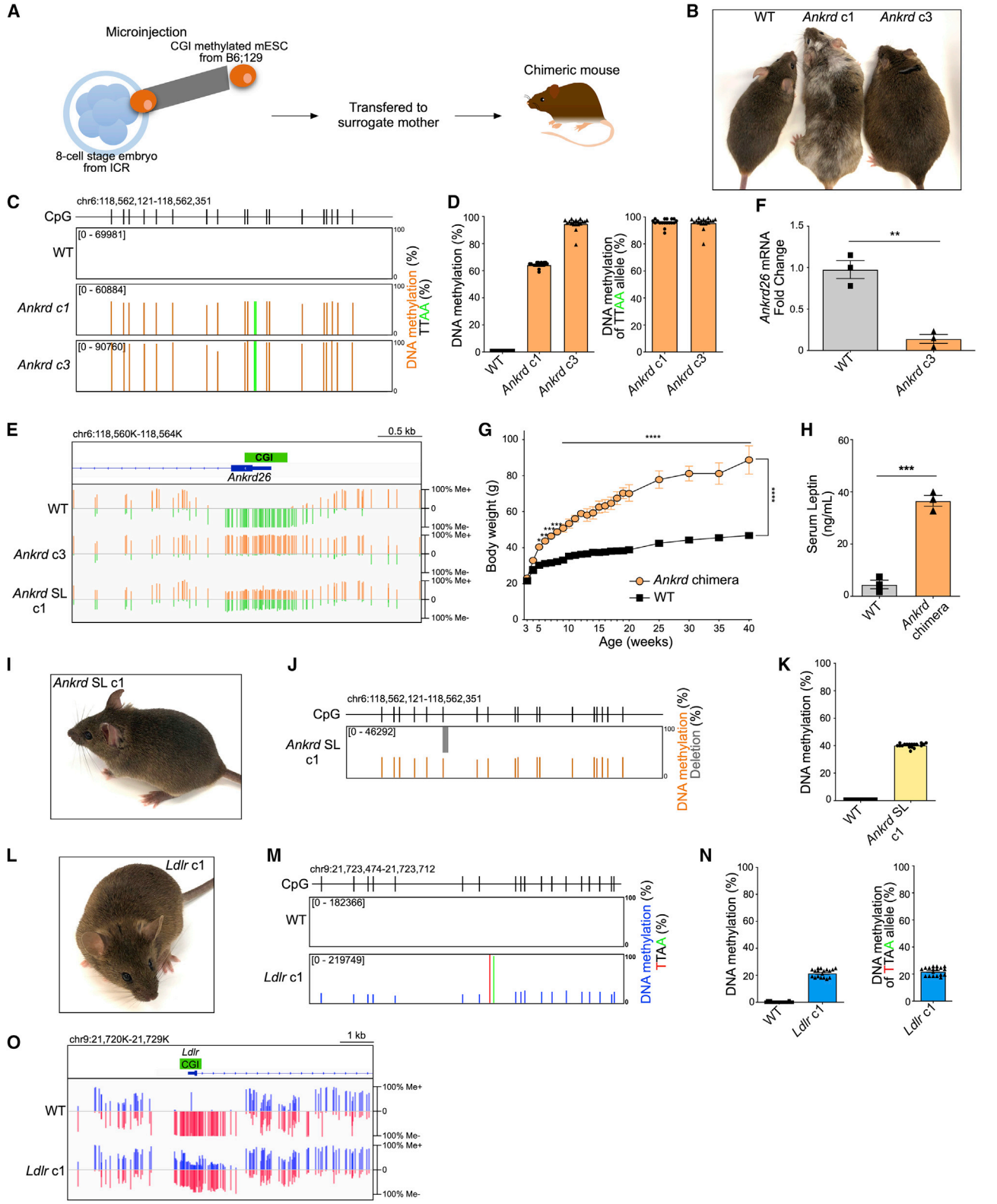

Figure 2. Generation of chimeric mice with DNA methylation of targeted CGI

(A) A schematic of generation of chimeric mice from DNA methylation-edited mESCs by microinjection.

(B) *Ankrd* c1, c3, and WT mouse at 10 months of age.

(legend continued on next page)

To investigate the stability of the acquired CGI methylation, we removed the CpG-free cassette by excision-only PiggyBac transposase, which recognizes the ITRs and TTAA sequences located at the end of the ITRs and subsequently removes the DNA between the two TTAA sequences. We first targeted similar sequences to TTAA in the CGIs of *Ankrd26* and *Ldlr*: TTCT and GTAC, respectively (Figures 1B and 1H). Thus, after integration and removal of the cassette, these two-point mutations, useful to distinguish targeted alleles from non-targeted (WT) alleles, remained. Following transient expression of the PiggyBac transposase in *Ankrd* HR clone number 1 (HR1) and *Ldlr* HR1, we handpicked individual clones and examined the DNA methylation status of the targeted CGIs by bisulfite sequencing analysis with next generation sequencing (NGS). After the cassettes were precisely excised, the HR excised (ex) clones exhibited TTAA at the targeted sites instead of TTCT or GTAC in *Ankrd26* CGI or *Ldlr* CGI, respectively (Figures 1B, 1D, 1H, 1I, S1D–S1F, and S2D–S2F). Moreover, both CGIs definitely exhibited an unmethylated status in untargeted WT ESCs, whereas the acquired DNA methylation of the targeted CGIs in the HR ex clones was retained: *Ankrd* HR1ex exhibited 85.2% methylation on *Ankrd26* CGI (Figures 1D and 1E) and *Ldlr* HR1ex exhibited 27.1% methylation on *Ldlr* CGI (Figures 1I and 1J). Targeted enrichment bisulfite sequencing analysis, which is able to reveal CpG methylation status at single-base resolution across about 10 kb region around targeted CGIs, confirmed that the methylation of the entire *Ldlr* CGI was retained (Figure 1K). These results indicate that the acquired methylations are stably maintained after removal of the cassette in mESCs. Moreover, in order to assess whether induction of DNA methylation is restricted to the targeted CGIs, we performed whole-genome bisulfite sequencing (WGBS) of the original mESC line, *Ankrd* HR1ex clone and *Ldlr* HR1ex clone. We detected the highest peak of acquired methylation at the targeted CGIs in both HRex clones and did not observe significant DNA methylation alterations at the neighboring loci (Figures 1F and S2G; Tables S1 and S2), indicating the high specificity of our approach.

Consistent with the methylation status, the expression of *Ankrd26* mRNA was repressed to 10% of WT levels in the HRex clone. This silencing remained even after 25 passages (Figure 1G). Furthermore, when we excised the cassette from the relatively low-methylated clone, *Ankrd* HR7 (Figure S1C), low DNA methylation levels on *Ankrd26* CGI (21.2%) and only modestly repressed mRNA levels were observed (Figures S1G and S1H). These data show that the expression of *Ankrd26* is repressed depending on the acquired DNA methylation of the CGI in *Ankrd* HR1ex, but not on the TTAA mutations. In addition, and to avoid generating point mutations, we targeted the endogenous TTAA sequence located 45 bp upstream of the above-described targeted site (TTCT) within the *Ankrd26* CGI. Through integration and removal of the cassette at the site on one allele (a deletion caused by Cas9 occurred on the other allele) (Figures 1C and S1I–S1N), the *Ankrd* seamless (SL) HR1ex clone exhibited 49.6% methylation on *Ankrd26* CGI (Figures 1C–1E). Thus, targeting the endogenous TTAA sequence induces stable DNA methylation without mutation.

Furthermore, by whole-genome sequence analysis, we confirmed the absence of unexpected mutations at 1 M (10^6) bp upstream and downstream of the targeted sites in the HRex clones (*Ankrd*HR1ex, *Ldlr*HR1ex, and *Ankrd*SLHR1ex) (Table S3) and did not detect any SNVs and indels at the potential off-target sites via Cas9 in genomes of these clones (Table S4).

Taken together, these data show that integration of CpG-free DNA induces *de novo* methylation of targeted CGIs in mESCs. Moreover, once DNA methylation is established across the targeted CGI, it is maintained, even after cassette excision and long-term culture of mESCs. Our approach through CpG-free DNA integration and excision by the PiggyBac transposase allows for the establishment of DNA methylation-edited mESCs, which retain stable DNA methylation of targeted CGIs, without altering genomic DNA sequence.

Generation of targeted DNA methylation-edited mice

To examine whether DNA methylation-edited mice can be generated from DNA methylation-edited ESCs, we microinjected 10–15 DNA methylation-edited mESCs, either *Ankrd* HR1ex, *Ankrd* HR7ex, *Ankrd* SL HR1ex, or *Ldlr* HR1ex, originally derived from a C57BL/6;129S hybrid male embryo, into recipient 8-cell stage embryos obtained from Institute of Cancer Research (ICR)(CD-1) mice, which have a white coat color, in order to detect chimerism by coat color (Figure 2A). We successfully generated high-level contribution chimeric male mice, *Ankrd* chimera (c) 1 to c3, from *Ankrd* HR1ex injection (Figure 2B). *Ankrd* c3 exhibited agouti coat color throughout the whole body, suggesting that the chimera is exclusively derived from the injected ESCs. This was also supported by NGS analysis of genomic DNA purified from tail-tip showing that 67% and 99% of mapped reads at the targeted site included the TTAA sequence in the chimeric mice *Ankrd* c1 and c3, respectively (Figure 2C). Importantly, 95% of CpGs in the *Ankrd26* CGI on the TTAA alleles were methylated in somatic cells of both adult chimeric mice (Figures 2C and 2D). This implies that the acquired DNA methylation of *Ankrd26* CGI in mESCs was maintained throughout mouse development. Targeted enrichment bisulfite sequencing analysis confirmed that although a WT mouse exhibited completely unmethylated *Ankrd26* CGI, *Ankrd* c3 exhibited the hypermethylation status of the entire *Ankrd26* CGI

(C, D, J, K, M, and N) Bisulfite sequencing analysis. (D, K, and N) Data represent mean ± SEM of methylation status of the 18 CpG sites in the CGIs. (D and N) Methylation status of whole mapped reads (left) and among reads of the TTAA alleles (right). See also Figure S3.
(E and O) Target enrichment-genome bisulfite sequencing analysis.
(F) Quantitative RT-PCR analysis of *Ankrd26* mRNA expression. Error bars indicate ± SEM of three independent experiments. Versus WT; $^{**}p < 0.005$ by unpaired Student's t test.
(G) Body weight of male *Ankrd* chimeras (n = 3) and male ICR WT mice (n = 3). Data are expressed as mean ± SEM. $^{****}p < 0.0001$, $^{***}p < 0.001$, $^{**}p < 0.01$, $^{*}p < 0.05$ by two-way ANOVA followed by Bonferroni correction.
(H) Serum leptin levels in WT mice (n = 3) and *Ankrd* chimeras (n = 3). Error bars indicate ±SEM. Versus WT; $^{***}p < 0.0005$ by unpaired Student's t test.
(I) *Ankrd* SL c1 mouse at 12 weeks of ages.
(L) *Ldlr* c1 mouse at 16 weeks of ages.

(Figure 2E). Consistent with the high methylation status, *Ankrd26* mRNA expression was notably repressed in somatic cells of the *Ankrd* c3 mouse (Figure 2F).

Ankrd26 knockout mice have been reported to develop hyperphagia, obesity, gigantism, and elevated serum leptin levels.[47,51] To examine whether the *Ankrd* chimeras exhibit these phenotypes, we analyzed the mice from the time of weaning until 10 months of age. The chimeric male mice were much heavier than WT male mice (Figures 2B and 2G). Moreover, the chimeras exhibited markedly elevated serum leptin levels at 4 months of age (Figure 2H), consistent with the phenotypes reported for the *Ankrd26* knockout mice.[47] Thus, these results indicate that the robust gene silencing elicited by *Ankrd26* CGI methylation maintenance during mouse development was linked to the phenotypes observed in the chimeras. Moreover, the *Ankrd* HR7 chimera mouse (c1) generated from the low-methylated clone *Ankrd* HR7ex did not exhibit *Ankrd26* gene silencing and obesity (Figures S3A–S3C), suggesting that the gene silencing and obese phenotype observed in *Ankrd* c3 were caused by the extreme hypermethylation of the *Ankrd26* CGI, but not by the TTAA mutation. In addition, we generated a high-level contribution chimera, *Ankrd* SL c1, by injecting the ESC line *Ankrd* SL HR1ex, in which *de novo* methylation was induced without remaining mutations. The chimeric mouse also maintained the methylation level of *Ankrd26* CGI on a targeted allele (Figures 2I–2K). Targeted enrichment bisulfite sequencing analysis confirmed the methylation of the entire *Ankrd26* CGI in *Ankrd* SL c1 (Figure 2E). Similar to the heterozygous knockout mice, the *Ankrd* SL c1 mouse had no obvious phenotype.

We also successfully generated a high-level contribution chimeric male from *Ldlr* HR1ex injection, *Ldlr* c1 (Figure 2L), in which 99% of mapped reads included the TTAA sequence (Figure 2M). Moreover, *Ldlr* CGI in the chimera exhibited 21.5% methylation, similar to the injected mESCs (Figures 2M and 2N). Targeted enrichment bisulfite sequencing analysis confirmed the methylation of the entire *Ldlr* CGI in *Ldlr* c1 (Figure 2O).

Together, these results indicate that our approach is able to generate DNA methylation-edited mice exhibiting stably maintained acquired methylation to targeted CGIs, and silencing of downstream genes.

Transgenerational inheritance of DNA methylation of the *Ankrd26* CGI

To determine whether CGI methylation of the DNA methylation-edited mice can be transmitted to the next generation, we mated the chimera, *Ankrd* c3, with an ICR female. All first-generation progeny (F1) that inherited a TTAA allele exhibited *Ankrd26* CGI methylation (Figures 3A, 3C, and S4A), indicating that *Ankrd26* CGI methylation is transmitted to the next generation through the germ line of a chimeric sire. As observed in *Ankrd* c3, *Ankrd26* CGIs of TTAA alleles in F1 mice were almost fully methylated (approximately 95%) (Figures 3C and S4A). Targeted enrichment bisulfite sequencing analysis confirmed inherited methylation of the entire *Ankrd26* CGI in a F1 mouse (Figure 3B). Furthermore, F1 mice from the low-methylated chimera *Ankrd* HR7c1 also inherited a TTAA allele and exhibited *Ankrd26* CGI methylation (around 25%) (Figures S3D–S3F). Thus, DNA methylation levels of *Ankrd26* CGI observed in somatic cells of the chimeras were retained in their offspring.

In addition, we showed that induced DNA methylation on *Ankrd26* CGI without changes in the DNA sequence is stably transmitted from the *Ankrd26* SL chimera to the offspring (Figures 3L, 3M, and S4H). This rules out the possibility that the TTCT to TTAA mutations cause DNA methylation of the *Ankrd26* CGI in offspring of the chimeras *Ankrd* c3 and *Ankrd* HR7. Together, these observations indicate that DNA methylation of CGI could be passed to the offspring through the germ line.

To determine if the inherited methylation of the *Ankrd26* CGI could be passed to the F2 generation, we mated either a methylated F1 male (individual number 3, F1-3) with an ICR female or a methylated F1 female (F1-10) with an ICR male. In both crosses, all F2 mice that inherited the TTAA allele exhibited DNA methylation in their *Ankrd26* CGI (Figures 3A, 3D, 3E, S4B, and S4C), indicating that the methylation of the *Ankrd26* CGI can be stably transmitted to the offspring through both paternal and maternal germ lines. Moreover, all F3 and F4 mice that inherited the TTAA allele exhibited DNA methylation of the *Ankrd26* CGI on the TTAA allele and a reduction of *Ankrd26* CGI methylation was not evident until the F4 generation (Figures 3A, 3F–3J, and S4D–S4G). The F4 descendants from F1-3 or F1-10 inherited the TTAA alleles through the male or female germ line, respectively. There were no significant differences between the male or female germ line on transmission of the DNA methylation status at the *Ankrd26* CGI until the F4 generation (Figure 3K). Likewise, *Ankrd26* CGI methylation from the *Ankrd26* SL chimera was transmitted to the F3 offspring through both paternal and maternal germ lines (Figures 3L–3O and S4H–S4J). Thus, our results indicate that the induced methylation of the *Ankrd26* CGI is stably inherited by subsequent generations through both paternal and maternal germ lines, regardless of mouse line and genome background (Figures S4K–S4P).

Transgenerational transmission of *Ldlr* CGI methylation

Next, to evaluate the extent to which the acquired *Ldlr* CGI methylation is passed to offspring, we crossed *Ldlr* c1 with ICR females. Although all F1 mice that inherited a TTAA allele from *Ankrd* c3 and *Ankrd* HR7 c1 exhibited *Ankrd26* CGI methylation (Figures 3 and S3), one-third of the F1 generation mice (8/24) from *Ldlr* c1 exhibited DNA methylation of the *Ldlr* CGI at the TTAA allele and the remaining F1 mice (16/24) harbored unmethylated TTAA alleles (Figures 4A, 4C, S5A, and S5B). Moreover, targeted enrichment bisulfite sequencing analysis confirmed inherited methylation of the entire *Ldlr* CGI in F1 progeny that exhibited methylation (Figure 4B). Moreover, as observed in the case of inheritance of *Ankrd26* CGI methylation, the methylation of *Ldlr* CGI can be stably transmitted to the F2 offspring through both paternal and maternal germ lines (Figures 4A, 4D, 4F, S5C, and S5E–S5H). Conversely, an F1-19 sire harboring an unmethylated TTAA allele mated with an ICR female resulted in all F2 offspring that inherited TTAA allele exhibiting no DNA methylation of their *Ldlr* CGI (Figures 4A, 4E, and S5D). This result eliminates the possibility that the remaining GTAC-to-TTAA point mutations induced the *Ldlr* CGI methylation in the methylated offspring. Furthermore, all offspring until F6 that inherited a TTAA allele from the methylated male F-13 and female F1-21

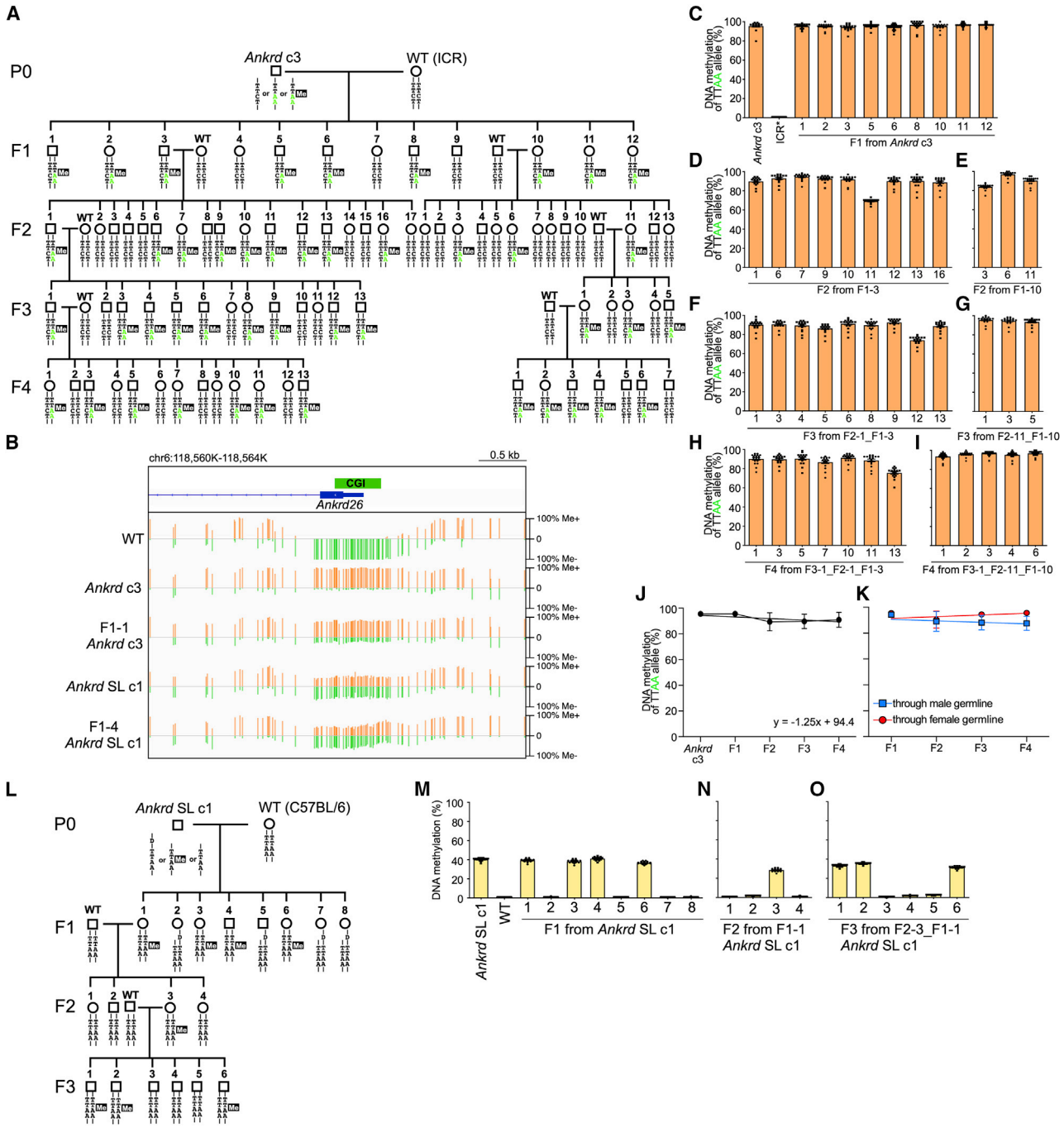

Figure 3. DNA methylation of *Ankrd26* CGI is inherited by the offspring

(A and L) Pedigrees of offspring from *Ankrd* c3 (A) and *Ankrd* SL c1 (L). Open circles and squares represent female and male mice, respectively. (A) TTCT and TTAA represent the WT and targeted alleles, respectively. (L) "D" represents alleles with the 4-bp deletion. Filled squares with "Me" represent DNA methylation of *Ankrd26* CGI.

(B) Target enrichment-genome bisulfite sequencing analysis.

(C–I and M–O) Bisulfite sequencing analysis. Data represent mean ± SEM of methylation status of the 18 CpG sites in *Ankrd26* CGI of TTAA allele (C–I) and of mapped reads (M–O). (C) ICR* shows the methylation status of whole reads. See also Figures S3 and S4.

(J and K) Bisulfite sequencing analysis showing changes of DNA methylation status of *Ankrd26* CGI on TTAA allele across generations. Data are expressed as mean ± SEM of the offspring in each generation.

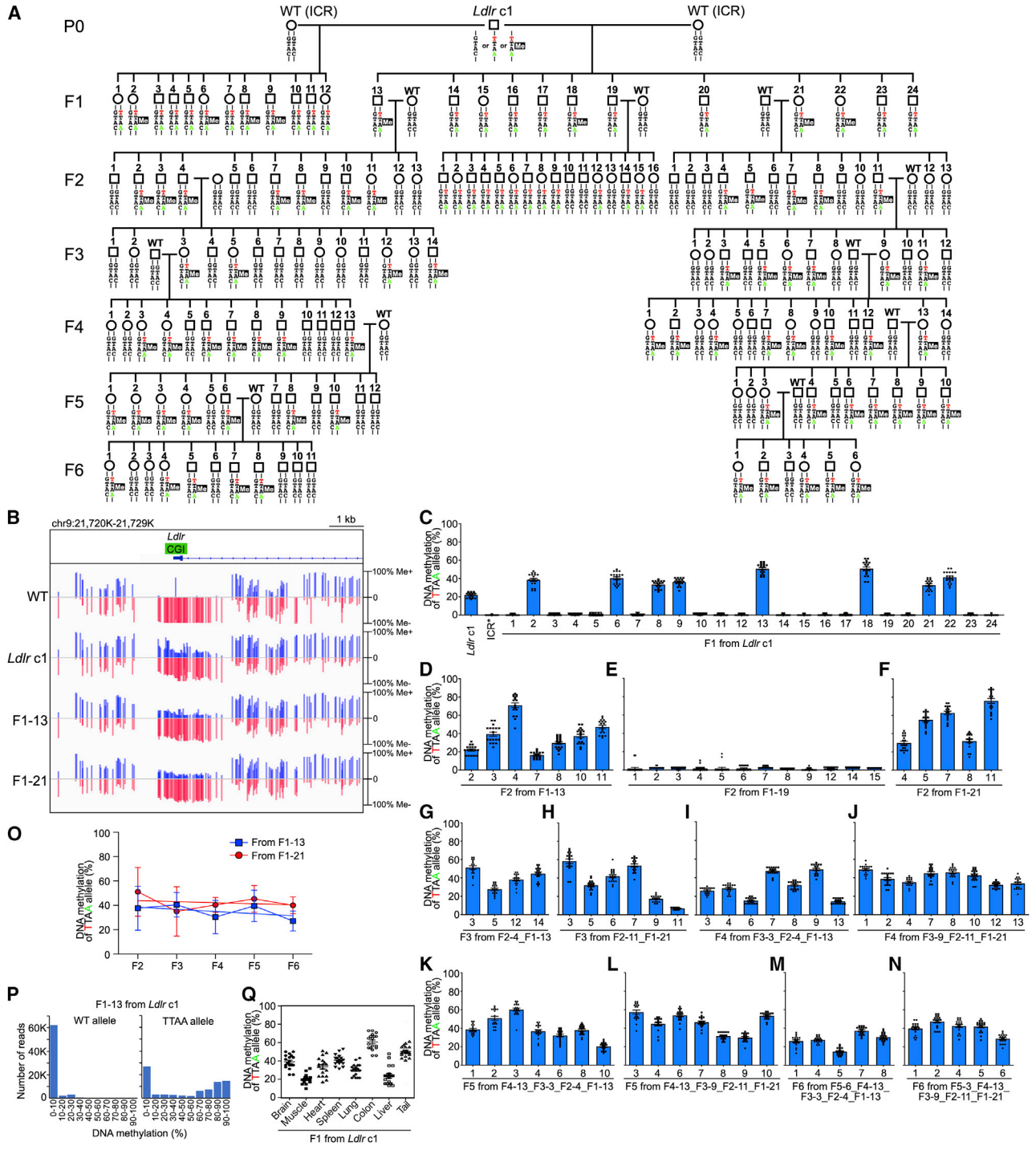

Figure 4. DNA methylation of *Ldlr* CGI is inherited by the offspring

(A) A pedigree of offspring from *Ldlr* c1.

(B) Target enrichment-genome bisulfite sequencing analysis.

(C–N and Q) Bisulfite sequencing analysis. Data represent mean ± SEM of methylation status of the 18 CpG sites in *Ldlr* CGI of TTAA allele. (C) ICR* shows the methylation status of whole reads. (Q) shows the methylation status of *Ldlr* CGI in various organs. See also Figure S5.

(O) Bisulfite sequencing analysis showing changes of DNA methylation status of *Ldlr* CGI on TTAA allele across generations. Data are expressed as mean ± SEM of the offspring in each generation.

(P) Distribution of reads by DNA methylation status. The bisulfite sequencing reads of F1-13 were sorted into two groups (WT allele or TTAA allele) and then were distributed by percentage of DNA methylation of each read.

exhibited DNA methylation of the *Ldlr* CGI on the TTAA allele (Figures 4G–4N and S5I–S5P). In both cases, a reduction in *Ldlr* CGI methylation was not evident until the F6 generation (Figure 4O). These results indicate that DNA methylation of the *Ldlr* CGI is stably inherited in subsequent generations.

Ldlr CGIs of TTAA alleles exhibited approximately 20%–70% methylation in methylated offspring from *Ldlr* c1, whereas *Ankrd26* CGIs of TTAA alleles in offspring from *Ankrd* c3 were almost fully methylated (approximately 95%). Based on the methylation status analysis of each NGS read, we found that in a methylated F1 male (F1-13) from *Ldlr* c1, approximately 40% of TTAA alleles were highly methylated (>70%), whereas half of the remainder were almost unmethylated (Figure 4P). These data suggest that the methylated F1 mice are mosaics of somatic cells in which *Ldlr* CGIs at TTAA alleles are either methylated or unmethylated. Various organs derived from different germ layers in a methylated F1 offspring exhibited a similar level of DNA methylation (Figures 4Q and S5Q), indicating that cell lineage-specific methylation was not observed. Moreover, distributions of NGS reads by *Ldlr* CGI methylation status in F2 and F3 offspring are similar to that of the F1-13 mouse (Figure S5R), suggesting that the allele which can reproduce the methylation mosaicism is passed to the next generation. A similar phenomenon was observed in single-cell re-cloning of methylated mESC clones. Although in the original *Ldlr* HR1ex clone, 20% of TTAA alleles were highly methylated and half of them were almost unmethylated, nine of ten re-clones exhibited a similar DNA methylation distribution with that of the original clone (Figures S2H–S2J), suggesting that regardless of whether an allele is methylated or unmethylated, every allele can reproduce the methylation distribution during propagation. In addition to the *Ldlr* CGI, in the F1-5 from the low-methylated chimera *Ankrd* HR7 c1, approximately 20% of TTAA alleles were highly methylated (>70%); 60% were almost unmethylated, and then, the F2 and F3 offspring inherited the distribution of methylation status from the F1-5 (Figure S3I). Although it remains unclear when the mosaicism occurs, these results suggest that the chromatin status at the targeted CGI, which can reproduce the methylation variants, may be stably transmitted across generations.

We did not obtain offspring with the unmethylated TTAA allele from methylated mice until the F6 generation with the exception of the F1 mice that inherited an unmethylated TTAA allele from *Ldlr* c1. The unmethylated TTAA allele from F1-19 also remained unmethylated after transmission to F2 mice (Figures 4E, 6F, and 6G). Thus, we did not observe a switching of DNA methylation status of the *Ldlr* CGI between generations after the F1 generation; from methylated to unmethylated *Ldlr* CGI and vice versa. Moreover, and in contrast with offspring from *Ldlr* c1, we did not observe F1 offspring with an unmethylated TTAA allele from the low-methylated *Ankrd* HR7 c1 (Figures S3D and S3F). Together, these data suggest the possibility that although we were supposed to establish a homogeneous cell clone, the injected cell clone *Ldlr* HR1ex may include two different lines of mESCs due to contamination: ESCs with alleles that can reproduce methylated TTAA and ESCs with stably unmethylated TTAA alleles. Indeed, we found that one of ten re-clones from *Ldlr* HR1ex clone had an unmethylated TTAA allele (Figures S2H–S2J). Thus, the chimera *Ldlr* c1 may be derived both from independent methylated and unmethylated mESC lines and, therefore, may be able to transmit both the methylated and unmethylated TTAA alleles to the F1 mice.

Transgenerational transmission of phenotypic traits via inheritance of *Ankrd26* CGI methylation

To determine whether gene silencing and chromatin status can also be transmitted to the offspring by the inheritance of a methylated *Ankrd26* CGI, we crossed a heterozygous methylated F1 male (F1-1) with a heterozygous methylated F1 female (F1-2) from the *Ankrd* c3 mouse. Subsequently, we crossed a homozygous F2 female (F2-6) with a homozygous F2 male (F2-8) (Figure 5A). The fully methylated *Ankrd26* CGI from *Ankrd* c3 was stably transmitted into both of the homozygous F2 and F3 mice, in which expression of *Ankrd26* mRNA was totally repressed (Figures 5B–5D, S4Q, and S4R). Consistently, ANKRD26 protein expression was not detected in homozygous F2 and F3 mice (Figure 5E). Moreover, and to determine whether chromatin status can also be transmitted, we examined the enrichment of histone H3K4me3 and H3K9me3 around the *Ankrd26* promoter associated with the CGI in the sibling WT and homozygous methylated mice by chromatin immunoprecipitation (ChIP)-qPCR assays. H3K4me3 is a hallmark of active gene promoter and H3K9me3 is associated with gene silencing. The high levels of H3K4me3 on the *Ankrd26* CGI observed in WT mice were highly diminished in both of the homo-methylated F2 and F3 mice, whereas the levels of H3K9me3 on the CGI were highly increased in the homozygous methylated mice (Figure 5F). These data indicate that consistent with the inherited DNA methylation of the *Ankrd26* CGI, gene silencing and a closed chromatin status on the *Ankrd26* promoter associated with the CGI were also transmitted to offspring. In addition, they were also transmitted to offspring independently of genetic sequence alterations in the *Ankrd* SL c1 line (Figures S4S, S4T, and S6A–S6D).

We then investigated whether the phenotypes observed in *Ankrd* chimeras can also be transmitted to the offspring. Consistent with inherited methylation of the *Ankrd26* CGI and gene silencing, homozygous methylated F3 male mice exhibited obese phenotypes (Figure 5G). Moreover, elevated serum leptin levels were observed in both F2 and F3 homozygous methylated mice (Figure 5H). These results indicate that the abnormalities caused by repression of *Ankrd26* expression are transmitted to the offspring. In contrast to the *Ankrd* c3 mouse line, homozygous F2 and F3 mice from the *Ankrd* HR7 chimera, which inherited the low-methylated *Ankrd26* CGI, did not exhibit *Ankrd26* gene silencing and obesity (Figures S3D–S3K). Taken together, our observations indicate that DNA methylation of the *Ankrd26* CGI passed from the highly methylated chimera, *Ankrd* c3, to the F3 offspring transmitted the phenotypes across generations.

Transgenerational transmission of hypercholesterolemia via inheritance of *Ldlr* CGI methylation

We next questioned whether gene silencing and phenotypes could be transmitted to the offspring by the inheritance of a methylated *Ldlr* CGI (Figure 6A). Again, all TTAA alleles inherited by F2 and F3 offspring exhibited methylation of the *Ldlr* CGI (Figures 6A, 6B, S5S, and S5T). Consistent with the methylation status, expression of *Ldlr* mRNA and LDLR protein was

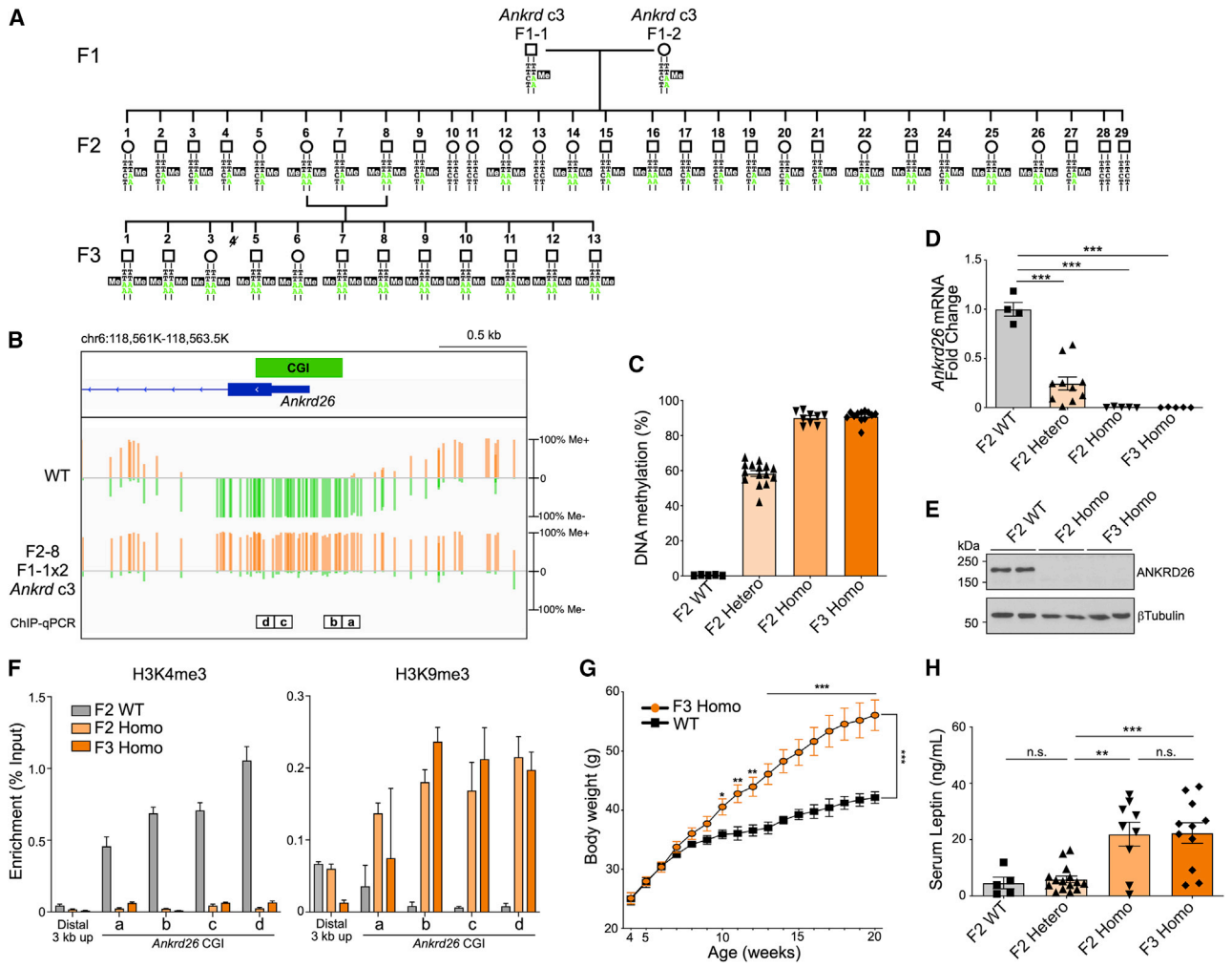

Figure 5. *Ankrd26* gene silencing and obesity are transmitted to the offspring

(A) A pedigree of offspring from *Ankrd* c3.

(B) Target enrichment-genome bisulfite sequencing analysis.

(C) Bisulfite sequencing analysis. Data are expressed as mean ± SEM of DNA methylation status of *Ankrd26* CGI in F2 and F3 offspring from *Ankrd* c3. See also Figure S4.

(D) Quantitative RT-PCR analysis of *Ankrd26* mRNA expression. Error bars indicate ± SEM. Versus WT; ***$p < 0.0001$ by unpaired Student's t test.

(E) Western blot analysis of mouse livers (n = 2) with anti-ANKRD26 antibody and anti-β-tubulin antibody.

(F) ChIP-qPCR analysis of H3K4me3 and H3K9me3 across *Ankrd26* CGI locus in the F2 (WT; n = 3, homo; n = 3) and F3 offspring (homo; n = 3) from *Ankrd* c3. Error bars indicate ±SD from triplicate experiments.

(G) Body weight of male F3 offspring (n = 8) and male WT mice (n = 8). Data are expressed as mean ± SEM. By two-way ANOVA followed by Bonferroni correction; ***$p < 0.0001$, **$p < 0.001$, *$p < 0.05$.

(H) Serum leptin levels in F2 and F3 offspring. Error bars indicate ± SEM. By unpaired Student's t test; **$p < 0.001$, ***$p < 0.0001$.

repressed in both F2 and F3 generations (Figures 6C and 6D). Conversely, the expression of *Ldlr* was not repressed in F3 mice that inherited unmethylated TTAA alleles from the F1-19 (Figures 6F–6H and S5U). These data indicate that gene repression via *Ldlr* CGI methylation is inherited by offspring. Consistently, the homozygous methylated mice in the F2 and F3 generation exhibited greatly elevated serum cholesterol levels (Figure 6E). Conversely, serum cholesterol levels of F3 mice that inherited unmethylated TTAA alleles from the F1-19 were similar to those of WT mice (Figure 6I). Taken together, our observations indicate that DNA methylation of the *Ldlr* CGI passed from the methylated chimera to the F3 offspring also transmitted the abnormal phenotype across generations.

DNA methylation of CGIs undergoes epigenetic reprogramming in the germ line and is reestablished in embryos

Given that there is bimodal and dynamic epigenetic reprogramming in PGCs and during early embryogenesis in mammals, our findings led us to question how the DNA methylation of CGIs is transmitted to the offspring. To start addressing this question,

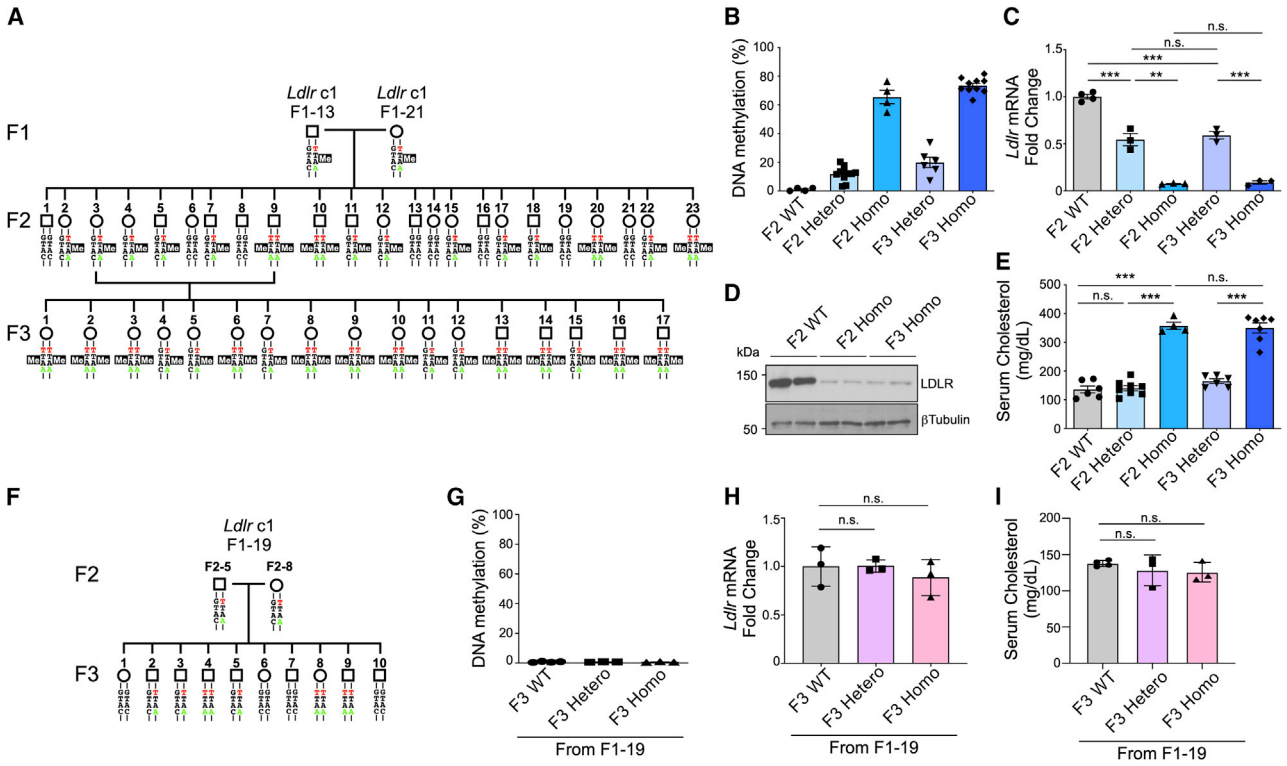

Figure 6. Hypercholesterolemia is transmitted to the offspring by inheritance of *Ldlr* CGI methylation

(A and F) Pedigrees of offspring from *Ldlr* c1.

(B and G) Bisulfite sequencing analysis. Data are expressed as mean ± SEM of DNA methylation status of *Ldlr* CGI in F2 and F3 offspring. See also Figure S5.

(C and H) Quantitative RT-PCR analysis of *Ldlr* mRNA expression. Error bars indicate ±SEM. By unpaired Student's t test; $^{**}p < 0.01$, $^{***}p < 0.001$.

(D) Western blot analysis of mouse livers (n = 2) with anti-LDLR antibody and anti-β-tubulin antibody.

(E and I) Serum cholesterol levels in offspring. Error bars indicate ±SEM. By unpaired Student's t test; $^{***}p < 0.0001$.

we first examined the DNA methylation status of the targeted CGIs in PGCs. In mice, genome-wide DNA demethylation starts in PGCs at around embryonic day 8.5 (E8.5), and the lowest level of global methylation (<10%) can be detected at E13.5.[21,22,52] We isolated PGCs by FACS sorting from E13.5 embryo gonads produced by crossing *Pou5f1*(Oct4)-driven GFP female mice, in which GFP is expressed in PGCs,[53] to a homogeneous *Ldlr* CGI-methylated male of the *Ldlr* c1 line (Figures 7A, S7A, and S7B) and performed bisulfite sequencing analysis of PGCs and somatic cells. Although somatic cells of the E13.5 embryos exhibited *Ldlr* CGI methylation on the TTAA allele inherited from the methylated sire, both male and female E13.5 PGCs barely exhibited DNA methylation on the *Ldlr* CGI (Figures 7B and S7C), indicating that the *Ldlr* CGI methylation inherited from the methylated male was erased during global DNA demethylation in PGCs until E13.5.

The demethylated whole-genome seen in PGCs undergoes *de novo* DNA methylation during spermatogenesis and oogenesis. We analyzed the *Ldlr* CGI methylation status in sperm isolated from cauda epididymis of methylated mice: the F1-13 and F1-18 from *Ldlr* c1 (Figure 7A). The *Ldlr* CGI methylation of the TTAA allele was almost undetectable in the sperm isolated from the F1 mice like that of PGCs (Figures 7C and S7D). Targeted enrichment bisulfite sequencing analysis confirmed the fully unmethylated status of the entire *Ldlr* CGI in the sperm of the F1-13 (Figure 7D). Similarly, oocytes from methylated female exhibited an extremely low level of methylation on the *Ldlr* CGI (Figures 7C and S7D). These data indicate that the DNA methylation of *Ldlr* CGI was demethylated during PGC development, and then, the unmethylated status of *Ldlr* CGI was maintained through differentiation into gametes in spite of global *de novo* methylation. More strikingly, given that all F2 offspring with the inherited TTAA allele from the F1 mice (F1-13, F1-18, and F1-21) exhibited *Ldlr* CGI methylation (Figures 4D, 4F, S5C, and S5E–S5H), these observations indicate that although sperm and oocyte carry the unmethylated *Ldlr* CGI allele to the zygote, *Ldlr* CGI methylation is reestablished in the offspring.

After fertilization, a loss of global DNA methylation starts and then continues until the blastocyst stage. Whole-genome DNA methylation is reestablished again in post-implantation embryos. To investigate when the erased DNA methylation of the *Ldlr* CGI is reestablished during embryogenesis, we examined the methylation status of the *Ldlr* CGI in E3.5 blastocysts and E6.5 epiblasts generated by crossing a homogeneously *Ldlr* CGI-methylated male mouse to WT female mice (Figure 7A). Although the blastocysts did not exhibit methylation of the *Ldlr* CGI at the TTAA allele, E6.5 epiblasts exhibited methylation of the *Ldlr* CGI (Figures 7E and S7E), indicating that methylation of the *Ldlr* CGI is

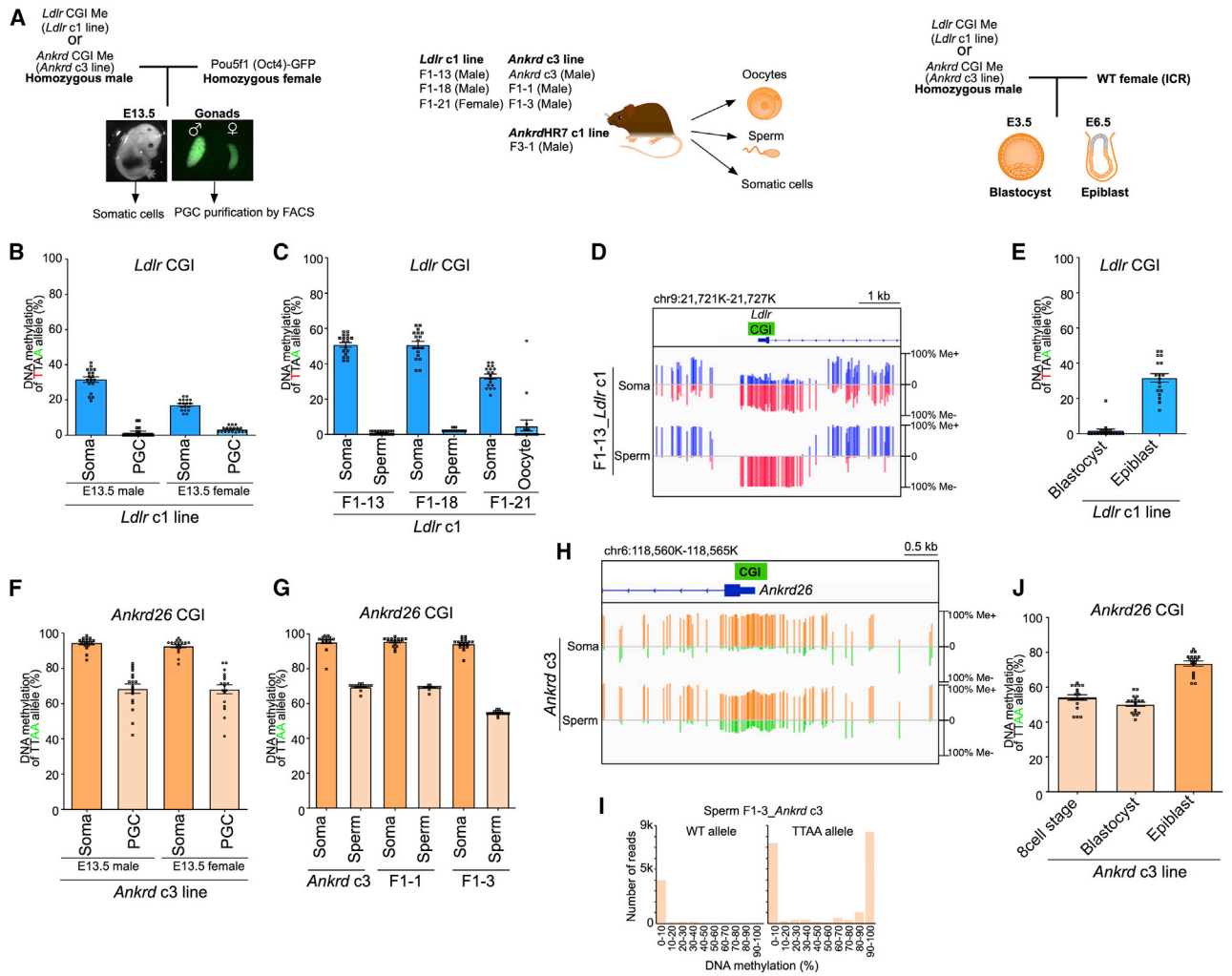

(legend on next page)

reestablished after implantation, when global genome methylation is established.

Taken together, these observations suggested that although DNA methylation itself on the *Ldlr* CGI can be erased in the germ line, the unmethylated sperm or oocytes from somatically methylated mice can transmit DNA methylation memory on the *Ldlr* CGI to the next generation and thereby reestablish DNA methylation of the *Ldlr* CGI in the offspring, resulting in transgenerational inheritance of *Ldlr* CGI methylation.

We then investigated the DNA methylation status of the *Ankrd26* CGI from *Ankrd* c3 in PGCs and early embryos. Although somatic cells from E13.5 male and female embryos exhibited almost fully methylated *Ankrd26* CGIs (>92%), male and female E13.5 PGCs exhibited 68.5% and 68.2% methylation of the *Ankrd26* CGI on the TTAA allele, respectively (Figures 7F and S7F). The same PGC samples exhibited a totally unmethylated status at the promoter of the germline-specific gene *Dazl*, which is normally unmethylated in the germ line and methylated in somatic cells[21] (Figure S7G), ruling out the possibility of somatic cell contamination in the PGC samples. These results indicated that although *Ankrd26* CGI methylation was partially demethylated during PGC development, methylation remained even after global DNA demethylation in PGCs.

Similar to the methylation status of the *Ankrd26* CGI in PGCs, sperm isolated from the offspring F1-1 and F1-3 from *Ankrd* c3 exhibited 69% and 55% methylation on the CGI of the TTAA allele, respectively (Figures 7G and S7H). Thus, the partially demethylated status of the *Ankrd26* CGI in E13.5 PGCs was maintained, but not increased, during spermatogenesis, when high levels of global DNA methylation are established. Consistent with this, targeted enrichment bisulfite sequencing analysis confirmed that sperm from *Ankrd* c3 and from males of the *Ankrd* SL c1 line exhibited a partially demethylated status of the entire *Ankrd26* CGI (Figures 7H and S7I). Interestingly, methylation levels of sperm from the F1-3 of *Ankrd* c3 line showed bimodal distribution; approximately half of TTAA alleles were highly methylated (>90%), whereas 44% of the alleles were almost unmethylated (Figures 7I and S7J). Given that all F2 offspring with the inherited TTAA allele from the F1-3 mouse exhibited *Ankrd26* CGI methylation (Figures 3D and S4B), these observations suggest that methylated sperm can transmit a methylated *Ankrd26* CGI to zygotes, and even unmethylated sperm may also transfer DNA methylation memory that can re-induce *de novo* methylation of the *Ankrd26* CGI in offspring.

At the blastocyst stage, when global DNA methylation levels are the lowest, the *Ankrd26* CGI on the TTAA allele exhibited 50.2% methylation (Figures 7J and S7K), showing that *Ankrd26* CGI methylation is resistant to global demethylation after fertilization. In epiblasts, the methylation levels of the *Ankrd26* CGI increase with the rise of global DNA methylation levels (Figures 7J and S7K).

In addition, we examined the methylation status of the *Ankrd26* CGI in sperm of offspring from *Ankrd*HR7 c1, whose somatic cells exhibit a low methylation pattern of the *Ankrd26* CGI (Figure S3). Although somatic cells exhibit 33.3% methylation of the *Ankrd26* CGI, the *Ankrd26* CGI methylation of the TTAA allele was barely detectable in sperm isolated from the mouse (Figure S7L), similar to the *Ldlr* CGI methylation observed in sperm from the offspring of *Ldlr* c1 rather than the *Ankrd26* CGI methylation in the sperm from the offspring of the highly methylated *Ankrd* c3 line. Thus, whether DNA methylation of the CGIs is totally erased, or partially demethylated and retained during global epigenetic reprogramming in PGCs, seems to be determined by the initial DNA methylation levels of the CGIs observed before global DNA demethylation, rather than by regions or *cis*-acting sequences. Therefore, although hyper methylation of CGIs, like methylation of the *Ankrd26* CGI from *Ankrd* c3, is not fully demethylated, hypomethylation of CGIs, like methylation of the *Ldlr* CGI from *Ldlr* c1 and *Ankrd26* CGI methylation from *Ankrd*HR7 chimera, can be totally erased once in the germ line. Importantly, in both of the cases, the DNA methylation levels observed on the CGIs before global epigenetic reprogramming are reestablished in embryos at early post-implantation stages, resulting in transmission of CGI methylation to the offspring (Figure 7K).

DISCUSSION

Transgenerational epigenetic inheritance is relatively common in plants and some invertebrates.[1–11] The possibility that this phenomenon may also occur in mammals was already formulated in ancient times by Hippocrates, later by Lamarck, Waddington, and others (see more recently[54–56]). However, despite the existence of some examples of heritable phenotypic variation, the lack of associated causality, together with the extensive reprogramming of the epigenome that takes place during early embryogenesis and development of the PGCs, argues against the idea of transgenerational epigenetic inheritance in mammals. By generating DNA methylation-edited mice, we show that acquired methylation of CGIs can be transmitted to offspring through the parental germ line in mice, thus supporting the concept that parental phenotypes can be transmitted to subsequent generations by inheritance of epigenetic information in mammals. Moreover, we found that the heritable DNA methylation of CGIs can be demethylated once in PGCs, suggesting that instead of DNA

Figure 7. The acquired CGI DNA methylation is demethylated in PGCs and then recovered in epiblast

(A) A schematic of sample preparation for PGCs, gametes, and early embryos.

(B, C, E, F, G, and J) Bisulfite sequencing analysis. Data represent mean ± SEM of methylation status of the 18 CpG sites in *Ldlr* CGI (B, C, and E) and *Ankrd26* CGI (F, G, and J) of TTAA allele. See also Figure S7.

(D and H) Target enrichment-genome bisulfite sequencing analysis.

(I) Distribution of reads by DNA methylation status. The bisulfite sequencing reads of sperm from the F1-3 were sorted into two groups (WT allele or TTAA allele) and then were distributed by percentage of DNA methylation of each read.

(K) A schematic showing dynamics of whole-genome DNA methylation and acquired DNA methylation of CGIs during mouse lifecycle. While endogenous CGIs always remain unmethylated, the acquired CGI methylation is stably maintained in somatic cells and is transmitted to the offspring. The CGI methylation can be demethylated in PGCs and then reestablished in epiblasts.

methylation, DNA methylation memory, elicited by as yet unidentified factors, is transmitted to the next generation.

Previous studies have shown that epimutations, changes in the chemical structure of DNA that does not change the DNA coding sequence, not only correlate with pathological alterations but may also have been correlated with disease and may be transmitted to offspring through the germ line.[35–37,57] Nonetheless, and despite many such observational studies, transgenerational epigenetic inheritance in humans has been challenged and dismissed because of the difficulties in ruling out the possibility that epimutation induction depends on genetic variants. In this study, we have addressed some of these issues by disentangling genetic and epigenetic inheritance using DNA methylation-edited mice, in which stable DNA methylation was induced at targeted CGI without genetic alteration, thereby demonstrating transgenerational inheritance of CGI methylation in mice. Moreover, we show that DNA methylation of the *Ankrd26* CGI passed to the F3 offspring transmitted the obese phenotype across generations. Downregulation of ANKRD26 and hyper-methylation of its promoter are common features of obesity in humans.[58] Together, given commonalities in biological systems between humans and mice, our findings may support the hypothesis that transgenerational inheritance of CGI methylation could take place in humans, and thus, it could contribute to heritable susceptibility to cancer, obesity, as well as other, so far unidentified, disease risks.

Although high-methylated CGIs, like *Ankrd26* CGI methylation from *Ankrd* c3, are not fully demethylated during genome-wide erasure of DNA methylation in PGCs, low-methylated CGIs, like methylation of the *Ldlr* CGI from *Ldlr* c1 and *Ankrd26* CGI methylation from *Ankrd*HR7 chimera, are totally erased once in the germ line (Figure 7). These observations are similar to the DNA methylation changes observed during retrotransposon silencing. In E13.5 PGCs, intracisternal A particles (IAPs), which is the most recently acquired transposon family in mouse genome and constantly highly methylated, are resistant to demethylation, whereas other elements such as long interspersed nuclear elements (LINEs) and short interspersed nuclear elements (SINEs) are almost invariably demethylated.[21,22] These data suggest both CGI methylation and retrotransposon methylation may share common demethylation mechanisms in PGCs. Conversely, unlike retrotransposon silencing, the DNA methylation of the targeted CGIs was not recovered during spermatogenesis. This could be explained by the fact that CGIs are not targeted by the small non-coding RNA PIWI-interacting RNA (piRNA), whereas the Piwi/piRNA complex binds to a retrotransposon through a complementary sequence and subsequently recruits DNA methylation machinery for silencing.[59,60]

Although all F2 offspring inherited the TTAA allele from the F1 males (F1-13 and F1-18) from the chimera *Ldlr* c1 exhibited *Ldlr* CGI methylation (Figures 4D, S5C, and S5F–S5H), sperm isolated from the F1 males did not exhibit *Ldlr* CGI methylation at the TTAA alleles (Figures 7C and S7D). We also found that methylation of the *Ldlr* CGI was reestablished at the epiblast stages (Figure 7E). In addition, although all F2 offspring inherited the TTAA allele from the F1-3 of the *Ankrd* c3 line exhibited methylation (Figure 3D), about half of the TTAA alleles of sperm from the F1-3 exhibited an almost fully unmethylated status (Figures 7G and 7I). These observations indicate that the DNA methylation of the CGIs can be erased once in the parental germ line and that even the unmethylated gametes can transmit DNA methylation memory of the CGIs to the zygote and thereby reestablish DNA methylation of the CGIs at the early post-implantation stage in the next generation. This elicits the question of what serves as DNA methylation memory? First, it is clear that the reestablishment of CGI methylation in post-implantation embryos is not dependent on the DNA sequence, unlike retrotransposon silencing, because the endogenous CGIs (before DNA methylation induction) remain unmethylated through all life stages. Besides DNA methylation, our approach may induce other stable epigenetic signatures or stable closed chromatin structure, which may function as a heritable epigenetic memory to reestablish DNA methylation of the CGI in offspring. This seems to be supported by the fact that when we only induced *de novo* DNA methylation at *Ankrd26* and *Ldlr* CGIs using the dCas9-DNA methyltransferase (DNMT) systems,[61,62] the acquired DNA methylation was not stably maintained in mouse ESCs (data not shown). Epigenetic marks, non-coding RNA and polycomb group proteins associated with heterochromatin, are possible candidates involved in generating DNA methylation memory. For example, in plants and fungi, it is common that *de novo* DNA methylation is directed by methylation of histone H3K9 and non-coding RNA.[63,64] The link between methylation of H3K9 and *de novo* DNA methylation has also been documented in mammals, in particular on retrotransposons.[65,66] However, like DNA methylation, other epigenetic marks should be subjected to dynamic epigenetic reprogramming in the germ line and after fertilization. The mechanisms underlying how heritable epigenetic memory is built in remain an interesting subject of study to be elucidated.

In conclusion, although the mechanistic details of the phenomenon here described need to await further experimentation, the capability of generating DNA methylation-edited mice may help to increase our knowledge on the physiological and pathological roles of CGI methylation, as well as to better understand the various natural and induced transgenerational phenomena observed in mammals and their physiological relevance. Looking from a wider lens, this knowledge may have implications on the role that epigenetic inheritance has in shaping some of the forces that drive macro-evolution, embryogenesis of mammals, and eventually as well, it may also lead to novel human health promoting strategies for future generations.

Limitations of the study

In addition to the *Ankrd26* and *Ldlr* CGIs described in here and four other CGIs in our previous work,[38] we also observed *de novo* and stable methylation at two other loci, the *Hsp90b* and *Mlh1* CGIs in PSCs. Nonetheless, a major question of the current study is the generalizability of the approach and the conclusions that can be drawn for different loci. Future efforts will be needed to ascertain whether natural and acquired DNA methylation at other CGIs as well as at other genomic regions with different features can be transmitted to offspring through the parental germ line.

STAR★METHODS

Detailed methods are provided in the online version of this paper and include the following:

SUPPLEMENTAL INFORMATION

Supplemental information can be found online at https://doi.org/10.1016/j.cell.2022.12.047.

ACKNOWLEDGMENTS

We dedicate this work to Jose Luis Mendoza, President of the UCAM, for having contributed to improving the lives of people and their descendants. We thank M. Sakurai, A. Sugawara, H. Matsuzaki, and K. Tanimoto for technical advice on generating chimeras; A. Nagy and F. Sugiyama for providing mESC lines; M. Shields for providing writing/editing/critical feedback; K. Matsusaka for advice on pathological examination; A. Fukamizu for discussion; Y. Hishida for experimental help; and M. Schwarz and P. Schwarz for administrative help.

AUTHOR CONTRIBUTIONS

Y.T. and J.C.I.B. conceived and designed the study. Y.T., M.M.V., K.T., C.F., and C.R.E. performed experiments in molecular biology. Y.T., Y.Y., and K.T. generated chimeras. Y.T., M.N.S., K.L., A.E.W., and Y.O. performed NGS data analysis. Y.T., M.K., K.S., F.H., and T.H. performed mice phenotypic analysis. E.N.-D. contributed to project design and characterization. Y.T. and J.C.I.B. prepared the manuscript.

DECLARATION OF INTERESTS

The authors declare no competing interests.

INCLUSION AND DIVERSITY

We support inclusive, diverse, and equitable conduct of research.

Received: April 2, 2022
Revised: August 19, 2022
Accepted: December 29, 2022
Published: February 7, 2023

REFERENCES

1. Bošković, A., and Rando, O.J. (2018). Transgenerational epigenetic inheritance. Annu. Rev. Genet. *52*, 21–41. https://doi.org/10.1146/annurev-genet-120417-031404.
2. Daxinger, L., and Whitelaw, E. (2012). Understanding transgenerational epigenetic inheritance via the gametes in mammals. Nat. Rev. Genet. *13*, 153–162. https://doi.org/10.1038/nrg3188.
3. Grossniklaus, U., Kelly, W.G., Kelly, B., Ferguson-Smith, A.C., Pembrey, M., and Lindquist, S. (2013). Transgenerational epigenetic inheritance: how important is it? Nat. Rev. Genet. *14*, 228–235. https://doi.org/10.1038/nrg3435.
4. Heard, E., and Martienssen, R.A. (2014). Transgenerational epigenetic inheritance: myths and mechanisms. Cell *157*, 95–109. https://doi.org/10.1016/j.cell.2014.02.045.
5. Horsthemke, B. (2018). A critical view on transgenerational epigenetic inheritance in humans. Nat. Commun. *9*, 2973. https://doi.org/10.1038/s41467-018-05445-5.
6. Jablonka, E., and Raz, G. (2009). Transgenerational epigenetic inheritance: prevalence, mechanisms, and implications for the study of heredity and evolution. Q. Rev. Biol. *84*, 131–176. https://doi.org/10.1086/598822.
7. Cavalli, G., and Heard, E. (2019). Advances in epigenetics link genetics to the environment and disease. Nature *571*, 489–499. https://doi.org/10.1038/s41586-019-1411-0.
8. Lim, J.P., and Brunet, A. (2013). Bridging the transgenerational gap with epigenetic memory. Trends Genet. *29*, 176–186. https://doi.org/10.1016/j.tig.2012.12.008.
9. Perez, M.F., and Lehner, B. (2019). Intergenerational and transgenerational epigenetic inheritance in animals. Nat. Cell Biol. *21*, 143–151. https://doi.org/10.1038/s41556-018-0242-9.
10. Radford, E.J. (2018). Exploring the extent and scope of epigenetic inheritance. Nat. Rev. Endocrinol. *14*, 345–355. https://doi.org/10.1038/s41574-018-0005-5.
11. Rechavi, O., and Lev, I. (2017). Principles of transgenerational small RNA inheritance in Caenorhabditis elegans. Curr. Biol. *27*, R720–R730. https://doi.org/10.1016/j.cub.2017.05.043.
12. Reik, W., and Walter, J. (2001). Genomic imprinting: parental influence on the genome. Nat. Rev. Genet. *2*, 21–32. https://doi.org/10.1038/35047554.
13. Saitou, M., Kagiwada, S., and Kurimoto, K. (2012). Epigenetic reprogramming in mouse pre-implantation development and primordial germ cells. Development *139*, 15–31. https://doi.org/10.1242/dev.050849.
14. Sasaki, H., and Matsui, Y. (2008). Epigenetic events in mammalian germ-cell development: reprogramming and beyond. Nat. Rev. Genet. *9*, 129–140. https://doi.org/10.1038/nrg2295.
15. Tang, W.W.C., Kobayashi, T., Irie, N., Dietmann, S., and Surani, M.A. (2016). Specification and epigenetic programming of the human germ line. Nat. Rev. Genet. *17*, 585–600. https://doi.org/10.1038/nrg.2016.88.
16. von Meyenn, F., and Reik, W. (2015). Forget the parents: epigenetic reprogramming in human germ cells. Cell *161*, 1248–1251. https://doi.org/10.1016/j.cell.2015.05.039.
17. Reik, W., Dean, W., and Walter, J. (2001). Epigenetic reprogramming in mammalian development. Science *293*, 1089–1093. https://doi.org/10.1126/science.1063443.
18. Guo, F., Yan, L., Guo, H., Li, L., Hu, B., Zhao, Y., Yong, J., Hu, Y., Wang, X., Wei, Y., et al. (2015). The transcriptome and DNA methylome landscapes of human primordial germ cells. Cell *161*, 1437–1452. https://doi.org/10.1016/j.cell.2015.05.015.

19. Hackett, J.A., SenGupta, R., Zylicz, J.J., Murakami, K., Lee, C., Down, T.A., and Surani, M.A. (2013). Germline DNA demethylation dynamics and imprint erasure through 5-hydroxymethylcytosine. Science *339*, 448–452. https://doi.org/10.1126/science.1229277.

20. Hajkova, P., Ancelin, K., Waldmann, T., Lacoste, N., Lange, U.C., Cesari, F., Lee, C., Almouzni, G., Schneider, R., and Surani, M.A. (2008). Chromatin dynamics during epigenetic reprogramming in the mouse germ line. Nature *452*, 877–881. https://doi.org/10.1038/nature06714.

21. Kobayashi, H., Sakurai, T., Miura, F., Imai, M., Mochiduki, K., Yanagisawa, E., Sakashita, A., Wakai, T., Suzuki, Y., Ito, T., et al. (2013). High-resolution DNA methylome analysis of primordial germ cells identifies gender-specific reprogramming in mice. Genome Res. *23*, 616–627. https://doi.org/10.1101/gr.148023.112.

22. Seisenberger, S., Andrews, S., Krueger, F., Arand, J., Walter, J., Santos, F., Popp, C., Thienpont, B., Dean, W., and Reik, W. (2012). The dynamics of genome-wide DNA methylation reprogramming in mouse primordial germ cells. Mol. Cell *48*, 849–862. https://doi.org/10.1016/j.molcel.2012.11.001.

23. Tang, W.W.C., Dietmann, S., Irie, N., Leitch, H.G., Floros, V.I., Bradshaw, C.R., Hackett, J.A., Chinnery, P.F., and Surani, M.A. (2015). A unique gene regulatory network resets the human germline epigenome for development. Cell *161*, 1453–1467. https://doi.org/10.1016/j.cell.2015.04.053.

24. Borgel, J., Guibert, S., Li, Y., Chiba, H., Schübeler, D., Sasaki, H., Forné, T., and Weber, M. (2010). Targets and dynamics of promoter DNA methylation during early mouse development. Nat. Genet. *42*, 1093–1100. https://doi.org/10.1038/ng.708.

25. Guo, H., Zhu, P., Yan, L., Li, R., Hu, B., Lian, Y., Yan, J., Ren, X., Lin, S., Li, J., et al. (2014). The DNA methylation landscape of human early embryos. Nature *511*, 606–610. https://doi.org/10.1038/nature13544.

26. Smith, Z.D., Chan, M.M., Mikkelsen, T.S., Gu, H., Gnirke, A., Regev, A., and Meissner, A. (2012). A unique regulatory phase of DNA methylation in the early mammalian embryo. Nature *484*, 339–344. https://doi.org/10.1038/nature10960.

27. Blewitt, M.E., Vickaryous, N.K., Paldi, A., Koseki, H., and Whitelaw, E. (2006). Dynamic reprogramming of DNA methylation at an epigenetically sensitive allele in mice. PLoS Genet. *2*, e49. https://doi.org/10.1371/journal.pgen.0020049.

28. Morgan, H.D., Sutherland, H.G., Martin, D.I., and Whitelaw, E. (1999). Epigenetic inheritance at the agouti locus in the mouse. Nat. Genet. *23*, 314–318. https://doi.org/10.1038/15490.

29. Saxonov, S., Berg, P., and Brutlag, D.L. (2006). A genome-wide analysis of CpG dinucleotides in the human genome distinguishes two distinct classes of promoters. Proc. Natl. Acad. Sci. USA *103*, 1412–1417. https://doi.org/10.1073/pnas.0510310103.

30. Bar, S., and Benvenisty, N. (2019). Epigenetic aberrations in human pluripotent stem cells. EMBO J. *38*, 3. https://doi.org/10.15252/embj.2018101033.

31. Curtin, K., Slattery, M.L., and Samowitz, W.S. (2011). CpG island methylation in colorectal cancer: past, present and future. Patholog. Res. Int. *2011*, 902674. https://doi.org/10.4061/2011/902674.

32. Hitchins, M.P. (2015). Constitutional epimutation as a mechanism for cancer causality and heritability? Nat. Rev. Cancer *15*, 625–634. https://doi.org/10.1038/nrc4001.

33. Robertson, K.D. (2005). DNA methylation and human disease. Nat. Rev. Genet. *6*, 597–610. https://doi.org/10.1038/nrg1655.

34. Widschwendter, M., Jones, A., Evans, I., Reisel, D., Dillner, J., Sundström, K., Steyerberg, E.W., Vergouwe, Y., Wegwarth, O., Rebitschek, F.G., et al. (2018). Epigenome-based cancer risk prediction: rationale, opportunities and challenges. Nat. Rev. Clin. Oncol. *15*, 292–309. https://doi.org/10.1038/nrclinonc.2018.30.

35. Chan, T.L., Yuen, S.T., Kong, C.K., Chan, Y.W., Chan, A.S., Ng, W.F., Tsui, W.Y., Lo, M.W., Tam, W.Y., Li, V.S., et al. (2006). Heritable germline epimutation of MSH2 in a family with hereditary nonpolyposis colorectal cancer. Nat. Genet. *38*, 1178–1183. https://doi.org/10.1038/ng1866.

36. Crépin, M., Dieu, M.-C., Lejeune, S., Escande, F., Boidin, D., Porchet, N., Morin, G., Manouvrier, S., Mathieu, M., and Buisine, M.-P. (2012). Evidence of constitutional MLH1 epimutation associated to transgenerational inheritance of cancer susceptibility. Hum. Mutat. *33*, 180–188. https://doi.org/10.1002/humu.21617.

37. Hitchins, M.P., Wong, J.J.L., Suthers, G., Suter, C.M., Martin, D.I.K., Hawkins, N.J., and Ward, R.L. (2007). Inheritance of a cancer-associated MLH1 germ-line epimutation. N. Engl. J. Med. *356*, 697–705. https://doi.org/10.1056/NEJMoa064522.

38. Takahashi, Y., Wu, J., Suzuki, K., Martinez-Redondo, P., Li, M., Liao, H.-K., Wu, M.-Z., Hernández-Benítez, R., Hishida, T., Shokhirev, M.N., et al. (2017). Integration of CpG-free DNA induces de novo methylation of CpG islands in pluripotent stem cells. Science *356*, 503–508. https://doi.org/10.1126/science.aag3260.

39. Carone, B.R., Fauquier, L., Habib, N., Shea, J.M., Hart, C.E., Li, R., Bock, C., Li, C., Gu, H., Zamore, P.D., et al. (2010). Paternally induced transgenerational environmental reprogramming of metabolic gene expression in mammals. Cell *143*, 1084–1096. https://doi.org/10.1016/j.cell.2010.12.008.

40. Fradin, D., Boëlle, P.-Y., Belot, M.-P., Lachaux, F., Tost, J., Besse, C., Deleuze, J.-F., De Filippo, G.D., and Bougnères, P. (2017). Genome-wide methylation analysis identifies specific epigenetic marks in severely obese children. Sci. Rep. *7*, 46311. https://doi.org/10.1038/srep46311.

41. Huypens, P., Sass, S., Wu, M., Dyckhoff, D., Tschöp, M., Theis, F., Marschall, S., Hrabě de Angelis, M.H., and Beckers, J. (2016). Epigenetic germline inheritance of diet-induced obesity and insulin resistance. Nat. Genet. *48*, 497–499. https://doi.org/10.1038/ng.3527.

42. King, S.E., and Skinner, M.K. (2020). Epigenetic transgenerational inheritance of obesity susceptibility. Trends Endocrinol. Metab. *31*, 478–494. https://doi.org/10.1016/j.tem.2020.02.009.

43. Somer, R.A., and Thummel, C.S. (2014). Epigenetic inheritance of metabolic state. Curr. Opin. Genet. Dev. *27*, 43–47. https://doi.org/10.1016/j.gde.2014.03.008.

44. Watkins, A.J., and Sinclair, K.D. (2014). Paternal low protein diet affects adult offspring cardiovascular and metabolic function in mice. Am. J. Physiol. Heart Circ. Physiol. *306*, H1444–H1452. https://doi.org/10.1152/ajpheart.00981.2013.

45. Wei, Y., Yang, C.-R., Wei, Y.-P., Zhao, Z.-A., Hou, Y., Schatten, H., and Sun, Q.-Y. (2014). Paternally induced transgenerational inheritance of susceptibility to diabetes in mammals. Proc. Natl. Acad. Sci. USA *111*, 1873–1878. https://doi.org/10.1073/pnas.1321195111.

46. Zhang, Y., Shi, J., Rassoulzadegan, M., Tuorto, F., and Chen, Q. (2019). Sperm RNA code programmes the metabolic health of offspring. Nat. Rev. Endocrinol. *15*, 489–498. https://doi.org/10.1038/s41574-019-0226-2.

47. Bera, T.K., Liu, X.-F., Yamada, M., Gavrilova, O., Mezey, E., Tessarollo, L., Anver, M., Hahn, Y., Lee, B., and Pastan, I. (2008). A model for obesity and gigantism due to disruption of the Ankrd26 gene. Proc. Natl. Acad. Sci. USA *105*, 270–275. https://doi.org/10.1073/pnas.0710978105.

48. Ishibashi, S., Brown, M.S., Goldstein, J.L., Gerard, R.D., Hammer, R.E., and Herz, J. (1993). Hypercholesterolemia in low density lipoprotein receptor knockout mice and its reversal by adenovirus-mediated gene delivery. J. Clin. Invest. *92*, 883–893. https://doi.org/10.1172/JCI116663.

49. Hackett, J.A., Dietmann, S., Murakami, K., Down, T.A., Leitch, H.G., and Surani, M.A. (2013). Synergistic mechanisms of DNA demethylation during transition to ground-state pluripotency. Stem Cell Rep. *1*, 518–531. https://doi.org/10.1016/j.stemcr.2013.11.010.

50. Pastor, W.A., Chen, D., Liu, W., Kim, R., Sahakyan, A., Lukianchikov, A., Plath, K., Jacobsen, S.E., and Clark, A.T. (2016). Naive human pluripotent cells feature a methylation landscape devoid of blastocyst or germline memory. Cell Stem Cell *18*, 323–329. https://doi.org/10.1016/j.stem.2016.01.019.

51. Acs, P., Bauer, P.O., Mayer, B., Bera, T., Macallister, R., Mezey, E., and Pastan, I. (2015). A novel form of ciliopathy underlies hyperphagia and

obesity in Ankrd26 knockout mice. Brain Struct. Funct. *220*, 1511–1528. https://doi.org/10.1007/s00429-014-0741-9.

52. Guibert, S., Forné, T., and Weber, M. (2012). Global profiling of DNA methylation erasure in mouse primordial germ cells. Genome Res. *22*, 633–641. https://doi.org/10.1101/gr.130997.111.
53. Yoshimizu, T., Sugiyama, N., De Felice, M.D., Yeom, Y.I., Ohbo, K., Masuko, K., Obinata, M., Abe, K., Schöler, H.R., and Matsui, Y. (1999). Germline-specific expression of the Oct-4/green fluorescent protein (GFP) transgene in mice. Dev. Growth Differ. *41*, 675–684. https://doi.org/10.1046/j.1440-169x.1999.00474.x.
54. Liu, Y. (2007). Like father like son. A fresh review of the inheritance of acquired characteristics. EMBO Rep. *8*, 798–803. https://doi.org/10.1038/sj.embor.7401060.
55. Bohacek, J., and Mansuy, I.M. (2015). Molecular insights into transgenerational non-genetic inheritance of acquired behaviours. Nat. Rev. Genet. *16*, 641–652. https://doi.org/10.1038/nrg3964.
56. Skvortsova, K., Iovino, N., and Bogdanović, O. (2018). Functions and mechanisms of epigenetic inheritance in animals. Nat. Rev. Mol. Cell Biol. *19*, 774–790. https://doi.org/10.1038/s41580-018-0074-2.
57. Sloane, M.A., Nunez, A.C., Packham, D., Kwok, C.T., Suthers, G., Hesson, L.B., and Ward, R.L. (2015). Mosaic epigenetic inheritance as a cause of early-onset colorectal cancer. JAMA Oncol. *1*, 953–957. https://doi.org/10.1001/jamaoncol.2015.1484.
58. Desiderio, A., Longo, M., Parrillo, L., Campitelli, M., Cacace, G., de Simone, S., Spinelli, R., Zatterale, F., Cabaro, S., Dolce, P., et al. (2019). Epigenetic silencing of the ANKRD26 gene correlates to the pro-inflammatory profile and increased cardio-metabolic risk factors in human obesity. Clin. Epigenet. *11*, 1–14. https://doi.org/10.1186/s13148-019-0768-0.
59. Aravin, A.A., Sachidanandam, R., Bourc'his, D., Schaefer, C., Pezic, D., Toth, K.F., Bestor, T., and Hannon, G.J. (2008). A piRNA pathway primed by individual transposons is linked to de novo DNA methylation in mice. Mol. Cell *31*, 785–799. https://doi.org/10.1016/j.molcel.2008.09.003.
60. Watanabe, T., Tomizawa, S., Mitsuya, K., Totoki, Y., Yamamoto, Y., Kuramochi-Miyagawa, S., Iida, N., Hoki, Y., Murphy, P.J., Toyoda, A., et al. (2011). Role for piRNAs and noncoding RNA in de novo DNA methylation of the imprinted mouse Rasgrf1 locus. Science *332*, 848–852. https://doi.org/10.1126/science.1203919.
61. Amabile, A., Migliara, A., Capasso, P., Biffi, M., Cittaro, D., Naldini, L., and Lombardo, A. (2016). Inheritable silencing of endogenous genes by hit-and-run targeted epigenetic editing. Cell *167*, 219–232.e14. https://doi.org/10.1016/j.cell.2016.09.006.
62. Nuñez, J.K., Chen, J., Pommier, G.C., Cogan, J.Z., Replogle, J.M., Adriaens, C., Ramadoss, G.N., Shi, Q., Hung, K.L., Samelson, A.J., et al. (2021). Genome-wide programmable transcriptional memory by CRISPR-based epigenome editing. Cell *184*, 2503–2519.e17. https://doi.org/10.1016/j.cell.2021.03.025.
63. Cam, H.P., Chen, E.S., and Grewal, S.I.S. (2009). Transcriptional scaffolds for heterochromatin assembly. Cell *136*, 610–614. https://doi.org/10.1016/j.cell.2009.02.004.
64. Zhao, Y., and Chen, X. (2014). Noncoding RNAs and DNA methylation in plants. Natl. Sci. Rev. *1*, 219–229. https://doi.org/10.1093/nsr/nwu003.
65. Li, H., Rauch, T., Chen, Z.-X., Szabó, P.E., Riggs, A.D., and Pfeifer, G.P. (2006). The histone methyltransferase SETDB1 and the DNA methyltransferase DNMT3A interact directly and localize to promoters silenced in cancer cells. J. Biol. Chem. *281*, 19489–19500. https://doi.org/10.1074/jbc.M513249200.
66. Matsui, T., Leung, D., Miyashita, H., Maksakova, I.A., Miyachi, H., Kimura, H., Tachibana, M., Lorincz, M.C., and Shinkai, Y. (2010). Proviral silencing in embryonic stem cells requires the histone methyltransferase ESET. Nature *464*, 927–931. https://doi.org/10.1038/nature08858.
67. Li, H., and Durbin, R. (2009). Fast and accurate short read alignment with Burrows–Wheeler transform. Bioinformatics *25*, 1754–1760. https://doi.org/10.1093/bioinformatics/btp324.
68. Blankenberg, D., Gordon, A., Von Kuster, G., Coraor, N., Taylor, J., and Nekrutenko, A.; Galaxy Team (2010). Manipulation of FASTQ data with Galaxy. Bioinformatics *26*, 1783–1785. https://doi.org/10.1093/bioinformatics/btq281.
69. Pedersen, B.S., Eyring, K., De, S., Yang, I.V., and Schwartz, D.A. (2014). Fast and accurate alignment of long bisulfite-seq reads. Preprint at arXiv. https://doi.org/10.48550/arxiv.1401.1129.
70. Krueger, F., and Andrews, S.R. (2011). Bismark: a flexible aligner and methylation caller for bisulfite-Seq applications. Bioinformatics *27*, 1571–1572. https://doi.org/10.1093/bioinformatics/btr167.
71. Langmead, B., Trapnell, C., Pop, M., and Salzberg, S.L. (2009). Ultrafast and memory-efficient alignment of short DNA sequences to the human genome. Genome Biol. *10*, R25. https://doi.org/10.1186/gb-2009-10-3-r25.
72. der Auwera, G.A.V., and O'Connor, B.D. (2020). Genomics in the cloud: using docker, GATK, and WDL, T.O. Media, ed.
73. Bae, S., Park, J., and Kim, J.-S. (2014). Cas-OFFinder: a fast and versatile algorithm that searches for potential off-target sites of Cas9 RNA-guided endonucleases. Bioinformatics *30*, 1473–1475. https://doi.org/10.1093/bioinformatics/btu048.
74. Akalin, A., Kormaksson, M., Li, S., Garrett-Bakelman, F.E., Figueroa, M.E., Melnick, A., and Mason, C.E. (2012). methylKit: a comprehensive R package for the analysis of genome-wide DNA methylation profiles. Genome Biol. *13*, R87. https://doi.org/10.1186/gb-2012-13-10-r87.

STAR★METHODS

KEY RESOURCES TABLE

REAGENT or RESOURCE	SOURCE	IDENTIFIER
Antibodies		
Anti-Histone H3 (tri methyl K4) antibody-ChIP Grade	abcam	Cat# ab8580; RRID: AB_306649
Anti-Histone H3 (tri methyl K9) antibody-ChIP Grade	abcam	Cat# ab8898; RRID: AB_306848
Anti-ANKRD26 antibody	Proteintech	Cat# 20035-1-AP; RRID: AB_11183053
Anti-LDLR antibody	Invitrogen	Cat# PA5-81434; RRID: AB_2788644
Anti-beta Tubulin antibody	Invitrogen	Cat# MA5-11732; RRID: AB_10990122
Bacterial and virus strains		
E. coli OmniMAX	Invitrogen	C854003
Chemicals, peptides, and recombinant proteins		
DMEM	Gibco	11960-044
Knockout Serum Replacement	Gibco	10828-028
Non-Essential Amino Acids (NEAA)	Gibco	11140-050
GlutaMAX	Gibco	35050-061
Penicillin_Streptomycin	Gibco	15140-122
Sodium Pyruvate	Gibco	11360-070
b-mercaptoethanol	Gibco	21985-023
Leukemia Inhibitory Factor (LIF)	ESGRO	ESG1107
Fetal bovine serum (FBS)	Gibco	10437-028
Accumax	Innovative Cell Technologies, Inc.	AM105
GENETICIN(G418)	Invitrogen	11811-023
Pregnant Mare Serum Gonadotropin (PMSG)	PROSPEC	HOR-272
Human Chorionic Gonadotoropin (hCG)	PROSPEC	HOR-250
KSOM Mouse Embryo Media	Sigma-Aldrich	MR-121-D
PD0325901	Selleck Chemicals	S1036
CHIR99021	Reagents Direct	27-H76
Trypsin-EDTA	Gibco	25-300-054
collagenase type IV	Gibco	17100017
Critical commercial assays		
P3 Primary Cell 4D-Nucleofector kit	Lonza	V4XP-3024
EZ DNA Methylation-Gold Kit	Zymo Research	D5006
TaKaRa EpiTaqTM HS (for bisulfite-treated DNA)	TaKaRa	R110B
NEBNext Ultra II Ligation Module	NEB	E7595L
SureSelectXT Methyl-Seq Target Enrichment	Agilent Technologies	G9651A
Leptin Mouse ELISA Kit	Invitrogen	KMC2281
Cholesterol Quantification Assay kit	Sigma-Aldrich	CS0005
Maxima First Strand cDNA Synthesis Kit	Thermo Fisher	EP0741
SsoAdvanced Universal SYBR Green Supermix	Bio-Rad	1725272
Deposited data		
Target enrichment-genome methyl sequencing data	This paper	GEO: GSE160847
WGS	This paper	GEO: GSE160847
WGBS	This paper	GEO: GSE160847

(*Continued on next page*)

Continued

REAGENT or RESOURCE	SOURCE	IDENTIFIER
Experimental models: Cell lines		
mouse ESC line (mm1)	This paper	N/A
MEF	C&M Lab Pro	20404114
MEF (DR4)	ATCC	SCRC-1045
Experimental models: Organisms/strains		
Mouse: C57BL/6J	The Jackson Laboratory	#000664
Mouse: 129S1/SvImj	The Jackson Laboratory	#002448
Mouse: B6;CBA-Tg(Pou5f1-EGFP)2Mnn/J	The Jackson Laboratory	#004654
Mouse: ICR (CD-1)	ENVIGO	#030
Mouse: *Ankrd* chimeras (c1 to c3)	This paper	N/A
Mouse: *Ankrd* HR7 c1	This paper	N/A
Mouse: *Ankrd* SL c1	This paper	N/A
Mouse: *Ldlr* c1	This paper	N/A
Oligonucleotides		
TruSeq-Compatible Duplex Y Adapter	IDT	N/A
Primers	This paper	Table S5
Recombinant DNA		
pCas9 GFP	Addgene	#44719
gRNA Cloning Vector	Addgene	#41824
pCpGfree-vitroNmcs	InvivoGen	pcpgvtn-mcsg2
The PB-CMV-MCS-EF1a-RedPuro Vector	System Bioscience	PB514B-2
Excision-only PiggyBac Transposase expression vector	System Bioscience	PB220PA-1
Ldlr CGI CpG-free targeting vector	This paper	N/A
Ankrd26 CGI CpG-free targeting vector	This paper	N/A
Ankrd26 CGI SL CpG-free targeting vector	This paper	N/A
Ldlr CGI gRNA vector	This paper	N/A
Ankrd26 gRNA vector	This paper	N/A
Ankrd26 SL gRNA vector	This paper	N/A
Software and algorithms		
bwameth	Pedersen, B. S., et al.	https://usegalaxy.org
FASTQ Groomer	Blankenberg, D., et al.	https://usegalaxy.org
Integrative Genomics Viewer (IGV_2.3.35 and _2.10.2)	Broad Institute and the Regents of the University of California	https://software.broadinstitute.org/software/igv/
BD FACSDiva 8.0.2	BD Biosciences	N/A
Bismark	Krueger, F, et al.	N/A
Bowtie	Langmead, B, et al.	N/A
Prism 9 (Version 9.3.1)	GraphPad	N/A
BWA	Li and Durbin	N/A
Picard MarkDuplicates	Broadinstitute	https://github.com/broadinstitute/picard
GATK's HaplotypeCaller and GenotypeGVCFs	Van der Auwera GA & O'Connor BD	N/A
Cas-OFFFinder	Bae et al.	http://www.rgenome.net/cas-offinder/

RESOURCE AVAILABILITY

Lead contact

Further information and requests for resources and reagents should be directed to and will be fulfilled by the lead contact, Juan Carlos Izpisua Belmonte (jcbelmonte@altoslabs.com).

Materials availability

All mouse lines and plasmids generated in this study are available from the lead contact with a completed Materials Transfer Agreement.

Data and code availability

- Target enrichment-genome bisulfite sequencing data, WGS data, and WGBS data have been deposited at GEO: GSE160847.
- This paper does not report original code.
- Any additional information required to reanalyze the data reported in this paper is available from the lead contact upon request.

EXPERIMENTAL MODEL AND SUBJECT DETAILS

Mice

All of the mice experiments were performed under the ethical guidelines of the Salk Institute. The animal protocols were reviewed and approved by the Salk Institute Institutional Animal Care and Use Committee. C57BL/6J (#000664), 129S1/SvImj (#002448), and B6;CBA-Tg(Pou5f1-EGFP)2Mnn/J (#004654) mice were purchased from The Jackson Laboratory. ICR (CD-1) (#030) mice were purchased from ENVIGO. The chimeric mice; *Ankrd* c1 to c3, *Ankrd* HR7 c1, *Ankrd* SL c1 and *Ldlr* c1, were generated by microinjection of the DNA methylation-edited mESC lines in our laboratory at the Salk Institute. For measurement of body weight, while WT male mice were allocated to control groups randomly, all of the male *Ankrd* chimeras were used (Figure 2G) and the F3 male offspring were allocated to experimental groups randomly (Figure 5G). Measurement of serum leptin concentration were performed with WT ICR male mice allocated to control groups randomly and the male *Ankrd* chimeras at 16 weeks of age (Figure 2H) and the F2 and F3 male/female offspring at 16 weeks of age (Figure 5H). For ChIP analysis and RT-qPCR, the offspring were allocated to experimental groups randomly. Measurement of serum cholesterol concentration were performed with the F2 and F3 male/female offspring at 12 weeks of age (Figures 6E and 6I). For qRT-PCR analysis of *Ankrd26* mRNA expression, the following offspring from *Ankrd* c3 were used: F2 WT; n=4, F2 Hetero; n=10, F2 Homo; n=5, F3 Homo; n=5 (Figure 5D). For analysis of serum leptin levels, the following offspring from *Ankrd* c3 were used: F2 WT; n=5, F2 Hetero; n=15, F2 Homo; n=9, F3 Homo; n=11 (Figure 5H). For qRT-PCR analysis of *Ldlr* mRNA expression (Figures 6C and 6H), the following offspring from *Ldlr* c1 were used: (C) F2 WT; n=4, F2 Hetero; n=3, F2 Homo; n=3, F3 Hetero; n=3, F3 Homo; n=3. (H) F3 WT; n=3, F3 Hetero; n=3, F3 Homo; n=3. For analysis of serum cholesterol levels (Figures 6E and 6I), the following offspring from *Ankrd* c3 were used: (E) F2 WT; n=6, F2 Hetero; n=8, F2 Homo; n=4, F3 Hetero; n=6, F3 Homo; n=7. (I) F3 WT; n=4, F3 Hetero; n=3, F3 Homo; n=3. Mice were housed under a 12-hour light/dark cycle with free access to food and water in a temperature controlled room (22°C) and bred in the animal facility of the Salk Institute.

Derivation and culture of mouse ESCs

The mouse ESC line (mm1) was established from the inner cell mass of a blastocyst that was obtained from a C57BL/6J female mouse mated with a 129S1/SvImj male mouse. Mouse ESCs were cultured on MEF in mESC medium containing DMEM (11960-044, Gibco), 20% Knockout Serum Replacement (10828-028, Gibco), 0.1 mM Non-Essential Amino Acids (NEAA) (11140-050, Gibco), 2 mM GlutaMAX (35050-061, Gibco), 100 U_μg/ml Penicillin_Streptomycin (Pen_Strep) (15140-122, Gibco), 1 mM Sodium Pyruvate (11360-070, Gibco), 0.1 mM β-mercaptoethanol (21985-023, Gibco), and 1 x 10⁴ U/ml Leukemia Inhibitory Factor (LIF) (ESG1107, ESGRO). Mouse ESCs were grown in a humidified atmosphere composed of 5% CO2 in air at 37°C and fed daily. Accumax (Innovative Cell Technologies Inc.) was used for passaging. The mouse ESC line (mm1) was derived from a male embryo. Sex was determined by genotyping PCR for *Sry* gene locus on the Y chromosome. Primers are shown in Table S5. MEFs were inactivated using g-irradiation and were cultured in DMEM (11960-044, Gibco) supplemented with 10% fetal bovine serum (FBS, Gibco, 10437-028), 0.1 mM NEAA, 2 mM GlutaMAX, 100 U_μg/ml Pen_Strep. MEF-feeder plates were prepared the day before mESC passaging.

METHOD DETAILS

Plasmids

The pCas9 GFP (#44719) and gRNA Cloning Vector (#41824) plasmids were purchased from Addgene. CpG-free promoter and neomycin resistance gene were cloned from pCpGfree-vitroNmcs (purchased from InvivoGen) as described previously.[38] The pCAGmCherry-gRNA vector was constructed from the gRNA Cloning Vector (#41824). The PB-CMV-MCS-EF1a-RedPuro Vector

(PB514B-2) and the Excision-only PiggyBac Transposase expression vector (PB220PA-1) were purchased from System Bioscience.

Construction of CpG-free targeting vector

The CpG-free neo cassette was cloned as described previously.[38] PCR was conducted with Prime STAR GXL enzyme (Takara). The primer sequence is shown in Table S5. Through the cloning, chemically competent the *E. coli* OmniMAX (Invitrogen) was used. PiggyBac 5'ITR_CpG-free neo cassette_3'ITR cloning: DNA fragments of PiggyBac 5' inverted terminal repeat (ITR) and 3'ITR were amplified by PCR from the PiggyBac backbone plasmid (PB514B-2). 5ITR_R and 3ITR_F primers include BamHI and MfeI sites, respectively, to generate the site for CpG-free cassette insertion between 5' and 3' ITR. Both fragments of the 5' and 3' ITR were cloned into pUC19 digested with BamHI and EcoRI using an In-Fusion HD cloning Kit (Takara). The CpG-free neo cassette that was then cut out from pUC19_CpG-free neo by BamHI and EcoRI was inserted between BamHI and MfeI, which was located at the middle of the ITRs of pUC19_5'-3'ITR. For the CpG-free targeting vector for *Ldlr* CGI and *Ankrd26* CGI: the fragments of 5' and 3' homology arms were cloned from genomic DNA of mESCs by PCR. The fragments of PiggyBac 5'ITR_CpG-free neo cassette_3'ITR were amplified by PCR from the cloned vector described above. These fragments of homology arms and 5'ITR-CpG-free-3'ITR were cloned into pUC19 digested with BamHI and EcoRI using an In-Fusion HD cloning Kit (Takara).

Construction of sgRNA expression vector

The target sequence was subcloned into pCAGmCherry-gRNA according to the following protocol (http://www.addgene.org/static/data/93/40/adf4a4fe-5e77-11e2-9c30-003048dd6500.pdf). The targeted sites are shown in Table S5.

Isolation of targeted clones

Mouse ESCs cultured on MEFs in mESC medium were dissociated into single cells by Accumax (ICT). 3-5 x 10^6 cells were nucleofected with the CpG-free targeting vector (25 μg), the gRNA and Cas9 expression vectors (5 μg) using a P3 Primary Cell 4D-Nucleofector kit (Lonza) and a 4D-Nucleofector (Lonza), and then replated on drug-resistant MEFs (DR4) (ATCC). On the next day, G418 (200 μg/ml; Invitrogen) was added to the medium to start antibiotic selection. After an additional 10-15 days, G418-resistant clones were handpicked, transferred onto 96-well MEF plates, and expanded for further characterization. Correct targeting was checked by genotyping PCR and southern blotting. Primers are shown in Table S5.

Excision of the CpG-free cassette

HR clones in which the PB CpG-free cassette was integrated into the targeted CGI were dissociated into single cells by Accumax (ICT). They were then transfected with the Excision-only PiggyBac Transposase expression vector using Lipofectamine 2000 Transfection Reagent (Thermo Fisher) and replated onto MEFs in mESC medium. After 10 days, clones were handpicked, transferred onto 96-well MEF plates, and expanded. The removal of the CpG-free cassette was verified by genotyping PCR and southern blotting.

Generation of chimeras

Female ICR mice were superovulated by intraperitoneal injection with PMSG (PROSPEC), followed by injection of hCG (PROSPEC) 48 hr later. After mating with male ICR mice, 2-cell stage embryos were collected at E1.5 from the oviduct and cultured in a droplet of KSOM medium (Sigma-Aldrich) under mineral oil (Sigma-Aldrich) in a humidified atmosphere composed of 5% CO2 in air at 37°C. After culturing for one day, 8-cell-stage embryos were transferred into a drop of KSOM and placed on an inverted microscope (Olympus) fitted with micromanipulators (Narishige). From 48 hr before injection, ESCs were cultured in mouse ESC medium with 2i (0.2 μM PD0325901 (Selleck Chemicals), 3 μM CHIR99021 (Reagents Direct)). ESCs to be injected were loaded into a blunt-end micropipette of 20-μm internal diameter that was connected to a manual hydraulic oil microinjector (Eppendorf). The embryos were secured by a holding pipette, and a Piezo Micro Manipulator (Prime Tech Ltd, Japan) was used to create a hole in the zona pellucida. Next, 10 to 15 ESCs were injected into the subzonal space of an 8-cell-stage embryo. The injected embryos were cultured in KSOM for one day and then transferred into the uteri of pseudopregnant ICR females that had previously mated with vasectomized males.

Bisulfite sequencing analysis for mouse ESCs, tissues, and sperm

For digestion, mouse tails, mouse embryonic limbs and mESCs were incubated in lysis buffer (10 mM Tris-HCl (pH7.5), 100 mM NaCl, 1 mM EDTA, 0.3% SDS) with proteinase K (5 U/ml, NEB) at 55°C for 5 hr. Sperm was obtained from the cauda epididymis and digested in the lysis buffer with 10 mM DTT. Genomic DNA was purified by Phenol/Chloroform/Isoamyl Alcohol (Ambion) and ethanol precipitation. Bisulfite conversion of genomic DNA (2 μg) was carried out using the EZ DNA Methylation-Gold Kit (Zymo Research) according to the manufacturer's protocol. Bisulfite PCR for *Ldlr* CGI or *Ankrd26* CGI was performed using Epi Taq HS (Takara) with the specific 5' phosphorylated primers (Bisul Ldlr IS NGS F and R2, Bisul Ankrd IS NGS F and R2) under the following conditions: 94°C for 3 min, 35 cycles (94°C for 30 s, 56°C for 30 s, 72°C for 30 s), and 72°C for 10 min. The primers are shown in Table S5. Following purification, a TruSeq-Compatible Duplex Y Adapter (IDT) containing a single index was ligated to both ends of the amplicons using a

NEBNext Ultra II Ligation Module (NEB). After agarose gel electrophoresis for the products, a desired length of DNA fragments was isolated from the gel and then amplified by PCR with P5 and P7 primers using PrimeStar GXL DNA Polymerase (Takara) under the following conditions: 98°C for 3 min, 9 cycles (98°C for 10 s, 58°C for 15 s, 68°C for 30 s), and 68°C for 5 min. The amplicons were purified using AMPure XP (BECKMAN COULTER). 96 samples were usually pooled to make a library for sequencing. Following sample pooling with 50% Phix, sequencing was conducted using an Illumina MiniSeq by SE300. Base calling was carried out using Illumina software, and read quality was confirmed using FastQC. The files were uploaded to the Galaxy server (https://usegalaxy.org/), and the format was adjusted using the FASTQ Groomer tool.[68] The reads were mapped to the mm10 genome using bwameth in Galaxy.[69] Bwameth analyzed the base-specific methylation percentages using a C-to-T converted version of the genome. Methylation status and TTAA percentage in the CGIs (*Ldlr* CGI; chr9: 21,723,474-21,723,712. *Ankrd26* CGI; chr6: 118,562,121-118,562,351. on mm10) were visualized using the Integrated Genome Viewer.

Bisulfite sequencing analysis for oocytes, PGCs, and early embryos

Mouse PGCs were isolated from E13.5 embryos of female Tg(Pou5f1-EGFP) mice mated with a homozygous methylated male mouse of *Ankrd* c3 line or of *Ldlr* c1 line. Embryonic sex was distinguished by gonad morphology. For embryonic PGCs, we pooled gonads from three embryos. For embryonic somatic cells, we pooled limbs from the same three embryos and purified gDNA as described above. Following digestion of gonads with collagenase type IV (1%, Gibco) and Trypsin-EDTA (0.05%, Gibco), PGCs were isolated depending on GFP intensity using BD Biosciences FACSAriaTM Fusion. Blastocysts were collected from ICR female mice that were superovulated by injection with PMSG and hCG mated with homozygous methylated male mouse of *Ankrd* c3 line or of *Ldlr* c1 line at E3.5. Epiblasts were collected from ICR female mice naturally mated with homozygous methylated male mouse of *Ankrd* c3 line or of *Ldlr* c1 line at E6.5. While fifteen to twenty of blastocysts were pooled, three of epiblasts were pooled. Oocytes were collected from superovulated female mouse of *Ldlr* c1 line. Twenty of oocytes were pooled. The isolated PGCs (15000 $\sim$ 20000 cells), pooled blastocysts, pooled epiblasts, and pooled oocytes were incubated with 20 μl of the lysis buffer at 55°C for 2 hr and 95°C for 10 min, and then 130 μl of the CT-conversion reagent of the EZ DNA Methylation-Gold Kit was added. Bisulfite-converted genomic DNA was then purified according to the manufacturer's protocol. For PGCs, we performed bisulfite PCR and preparation of a sequencing library as described above. For early embryos and oocytes, nested PCR was carried out to amplify specific loci from bisulfited gDNA. *Ldlr* CGI or *Ankrd26* CGI was amplified using Epi Taq HS (Takara) with the specific 5' phosphorylated primers (For *Ldlr* CGI; 1st: Bisul Ldlr IS NGS F and R1, 2nd: Bisul Ldlr IS NGS F and R2, For *Ankrd26* CGI; 1st: Bisul Ankrd IS NGS F and R1, 2nd: Bisul Ankrd IS NGS F and R2) under the following conditions: 1st: 94°C for 3 min, 35 cycles (94°C for 30 s, 56°C for 30 s, 72°C for 30 s), and 72°C for 10 min, and 2nd: same condition through 30 cycles. One μl of the 1st PCR product was used for the nested (2nd) PCR. The primers are shown in Table S5. Adopter ligation and preparation of a sequencing library were performed as described above.

Target enrichment-genome bisulfite sequencing analysis

Target enrichment-genome methyl sequencing was performed as described previously[38] using the SureSelectXT Methyl-Seq Target Enrichment System for Illumina Multiplexed Sequencing (Agilent Technologies). The sequencing was performed with a customized capture library according to manufacturer's protocol. The biotinylated RNA capture probe library to capture specific genomic loci was designed to include three loci on the mouse genome: mm10, chr6:118556982-118565982, chr9:111265293-111280293, and chr9:21720056-21729056. Next, 3 μg of genomic DNA was sheared to 150 to 180-bp fragments using Covaris M220. Following hybridization between sheared DNA and the capture library, the captured genomic DNA was purified using streptavidin beads. Bisulfite conversion of the captured DNA was performed using the EZ DNA Methylation-Gold Kit (Zymo Research). Following indexing and sample pooling with 10% PhiX, sequencing was conducted using an Illumina NextSeq500 at PE150. Bisulfite sequencing reads were checked for read quality using FastQC and aligned to the mm10 genome with Bismark.[70] Bismark uses a C-to-T converted version of the genome and Bowtie alignment[71] (with a maximum of 1 seed mismatch allowed) to identify base-specific methylation percentages. CGIs were defined by the UCSC genome Browser.

The GEO accession number of the target enrichment-genome bisulfite sequencing analysis is "GSE160847".

Whole genome sequencing and analysis

Genomic DNA was purified from the original WT mESC (mm1), *Ankrd* HR1ex, *Ankrd* SL HR1ex, and *Ldlr* HR1ex clones using DNeasy Blood & Tissue Kits (Qiagen). Sequencing was conducted using Illumina NovaSeq at PE150 in Novogene Company (Beijing, China). Total 340.8 gigabytes of raw data were generated, yielding a median sequencing depth of 34 per genome. Raw WGS results were aligned at Novogene using BWA.[67] PCR duplicates were marked using Picard MarkDuplicates (https://github.com/broadinstitute/picard), and SNPs were called with GATK's HaplotypeCaller and GenotypeGVCFs.[72] SNPs were hard-filtered with vcftools using the following thresholds: –max-missing 0.5—mac 2—min-meanDP 15—minQ 30. Indels were called via a similar pipeline, but indel realignment and BQSR were performed in GATK before variant calling. Goldset mm10 indels for indel realignment and BQSR were downloaded from sanger.ac.uk. The following criteria were applied to remove false positive variants from the candidate variants called by GATK and obtain bonafide variants, including SNVs and Indels; we removed 1) coincident variants between *Ldlr* and *Ankrd* clones, 2) variants in repeated sequence, and 3) variants in more than 6 consecutive nucleotides sequence. We then removed false positive variants by visual inspection of mapped reads in BAM files with IGV. Finally, we

determined whether the bonafide variants are designed or unexpected variants. The raw data and the processed data have been deposited at GEO: GSE160847.

The potential Cas9-induced off-target cleavage sites, which contain up to three mismatches with the sgRNAs, were searched by Cas-OFFFinder.[73] We then examined whether there are SNVs and Indels around the potential off-target sites by visual inspection of mapped reads in BAM files with IGV.

Whole genome bisulfite sequencing and analysis

Genomic DNA was purified from the original WT mESC (mm1), *Ankrd* HR1ex, and *Ldlr* HR1ex clones using DNeasy Blood & Tissue Kits (Qiagen). Sequencing was conducted using Illumina NovaSeq at PE150 in Novogene Company (Beijing, China). Total 216.64 gigabytes of raw data were generated, yielding a median sequencing depth of 28 per genome. Raw WGBS results were aligned at Novogene using Bismark.[70] Bismark reports were analyzed in R with the methylKit package v.1.10.0.[74] The results were filtered by coverage to remove sites with fewer than 10 reads and sites above the 99.9th percentile for coverage, normalized, and pooled into 25bp tiles. Differential methylation was calculated with the getMethylDiff() function. The loci indicating p-value less than e^-10 were listed in Tables S1 and S2. The BAM files were visualized by IGV.

Quantitative RT-PCR

TRIZOL (Invitrogen) was used to extract total RNA from mouse ESCs and mouse tissues. To examine mRNA expression of *Ldlr*, we collected perfused mouse livers from offspring of *Ldlr* c1 line at 4∼5 months of age. For test of *Ankrd26* mRNA expression, total RNA was isolated from tails from offspring of *Ankrd* c3 line. cDNA was synthesized using a Maxima First Strand cDNA Synthesis Kit (Thermo Fisher). Quantitative RT-PCR was performed with SsoAdvanced Universal SYBR Green Supermix (Bio-Rad) using CFX384 Real-Time PCR Detection Systems (Bio-Rad). The expression levels of each gene were normalized to *Gapdh* and calculated using the ΔΔCT method. The primers are shown in Table S5.

Western Blot analysis

Perfused mouse livers were dissected. The pieces of livers were homogenized in a dounce homogenizer with lysis buffer (1xPBS, 1% NP40, 0.5% sodium deoxycholate, 0.1%SDS, with protease inhibitor cocktail (Santa Cruz)). 40 μg of total protein was mixed with SDS sample buffer and separated on SDS PAGE gel. A protein is transferred to PVDF membrane and then membrane was incubated with antibody at 4°C overnight. Detection was performed using HRP conjugated 2nd antibody and substrates.

Leptin quantification assay

Blood samples were collected by submandibular bleeding method from 16-weeks-old mice in the non-fasted state. Quantitative measurement of serum leptin was carried out using a Leptin Mouse ELISA kit (Invitrogen) according to the manufacturer's protocol. The standards and the samples in wells of the ELISA plate were incubated for 2 hours at 37°C. Following wash, we added the Leptin-biotin conjugate solution and the Streptavidin-HRP. For the assay, we read the absorbance at 450 nm.

Cholesterol quantification assay

Blood samples were collected by submandibular bleeding method from 12-weeks-old mice in the non-fasted state. Serum total cholesterol (which constitutes both free cholesterol and cholesteryl esters) was quantified using a Cholesterol Quantification Assay kit (Sigma-Aldrich) according to the manufacturer's protocol. We mixed the standards and the samples with the reaction mix, containing the probe and the enzyme, and incubate for 30 minutes at 37°C. For the assay, we measured fluorescence intensity at λ_{ex} = 535 nm/ λ_{em} = 587 nm.

Mouse liver ChIP-qPCR

ChIP-qPCR was carried out as described previously with modifications.[38] In brief, following liver perfusion with PBS, liver was fixed with 1% formaldehyde (Sigma-Aldrich) for 10 min and then quenched with glycine for 5 min. After rinse with PBS, the pieces of fixed liver were homogenized in a dounce homogenizer. Chromatin was isolated in lysis buffer (1xPBS, 1% NP40, 0.5% sodium deoxycholate, 0.1%SDS, with protease inhibitor cocktail (Santa Cruz)) and was sonicated using Covaris M220 to achieve 200–500 bp size chromatin fragments. Solubilized chromatin was immunoprecipiated with antibody against H3K4me3 (Abcam 8580) or H3K9me3 (Abcam 8898) overnight at 4°C. Antibody–chromatin complexes were pulled down using Dynabeads protein A (Invitrogen), washed and then eluted. After cross-linking reversal, RNase and proteinase K treatment, immunoprecipiated DNA was purified using AMPure beads (Beckman Coulter). To calculate the percent of input, quantitative real time PCR was performed with primers shown in Table S5.

Southern blot analysis

Southern blot analysis was performed as described previously.[38] To this end, 10 μg of genomic DNA for each sample was digested with 50 U restriction enzyme overnight and then subjected to electrophoresis for 3 h at 50 V on a 0.8% agarose gel. The gel was subsequently incubated in depurination buffer (0.25 M HCl) for 10 min and in denaturation buffer (1.5 M NaCl, 0.5 M NaOH) for 30 min, followed by incubation in neutralization buffer (0.5 M Tris-HCl [pH 7.4], 1.5 M NaCl). The DNA was

then blotted overnight onto a nylon membrane (positively charged)(Roche) by capillary transfer in 20 x SSC buffer. Probe hybridization and signal detection were performed according to the protocol of the DIG high prime DNA labeling and detection kit II (Roche). The probes were cloned from mouse genomic DNA by PCR with the primers shown in Table S5.

QUANTIFICATION AND STATISTICAL ANALYSIS

Statistical analyses were carried out using Prism 9 (Version 9.3.1) Software (GraphPad). Statistical parameters including statistical analysis, statistical significance, and n value are reported in the Figure legends. Statistical comparisons between two groups were made by unpaired Student's t-test. Two-way ANOVA followed by Bonferroni correction was used for comparisons of body weight.

Supplemental figures

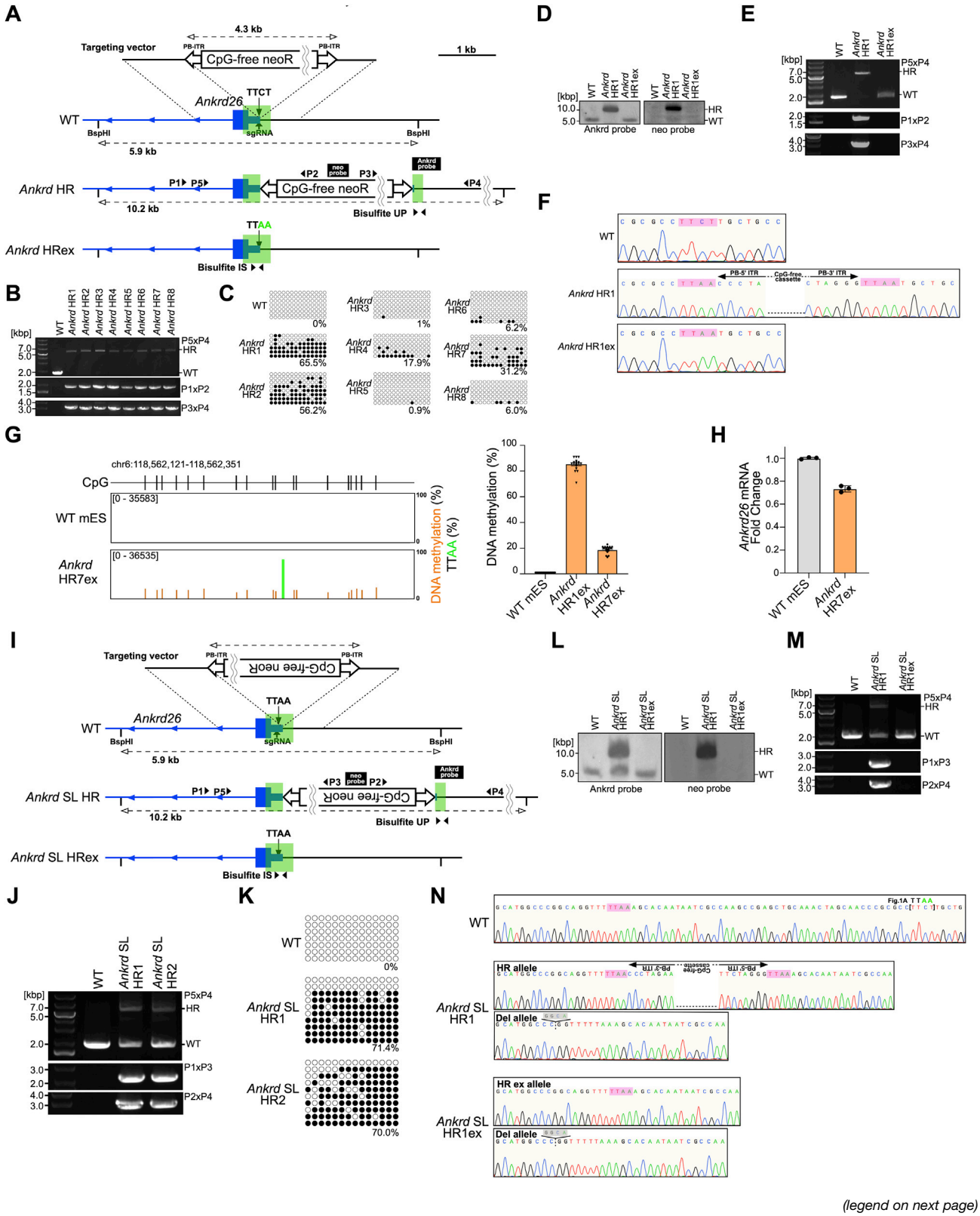

(legend on next page)

Figure S1. *Ankrd26* CGI methylation established by integration of CpG-free DNA in mESCs, related to Figure 1

(A and I) Schematics of integration of CpG-free DNA into (A) the TTCT site and (I) the TTAA site within *Ankrd26* CGI through HR and removal of the cassette in mESCs. Filled arrowheads represent PCR primers. Black bars with "probe" inside represent probes for southern blot analysis. Green boxes represent CpG island of *Ankrd26*.

(B and J) Genotyping of (B) the *Ankrd* HR and (J) *Ankrd* SL HR clones and the primers for PCR are shown in (A) and (I), respectively.

(C and K) Bisulfite sequencing analysis of upstream region of CpG-free DNA integration site within *Ankrd26* CGI and the primers for PCR are shown in (A) and (I), respectively.

(D and L) Southern blot analysis of WT, (D) *Ankrd* HR1, *Ankrd* HR1ex, and (L) *Ankrd* SL HR1, and *Ankrd* SL HR1ex clones. Genomic DNA was digested with BspHI. Targeted regions were detected by Ankrd probe (left) or *neo* probe (right). The probes are shown in (A) and (I).

(E and M) Genotyping of (E) the *Ankrd* HR1 and *Ankrd* HR1ex clones and (M) *Ankrd* SL HR1, and *Ankrd* SL HR1ex clones. The primers for PCR are shown in (A) and (I).

(F and N) Genomic DNA sequence of HR site in WT, (F) *Ankrd* HR1, *Ankrd* HR1ex, and (N) *Ankrd* SL HR1, *Ankrd* SL HR1ex clones. (F) Pink boxes represent the WT sequence, TTCT, and the sequence after targeting, TTAA. (N) Pink and gray boxes represent the targeted sequence, TTAA, and the 4 bp deletion, respectively. Brackets include the targeted sequence, TTCT, shown in Figures 1B and S1A–S1F.

(G) Bisulfite sequencing analysis showing DNA methylation status of *Ankrd26* CGI. (Left) Each bar represents the methylation status of a single CpG site or percentage of TTAA. Number of mapped reads is shown in the columns. (Right) Data represent mean ± SEM of methylation status of the 18 CpG sites in the CGIs.

(H) Quantitative RT-PCR analysis of *Ankrd26* mRNA expression normalized to *Gapdh* mRNA. Error bars indicate ±SEM of three independent experiments.

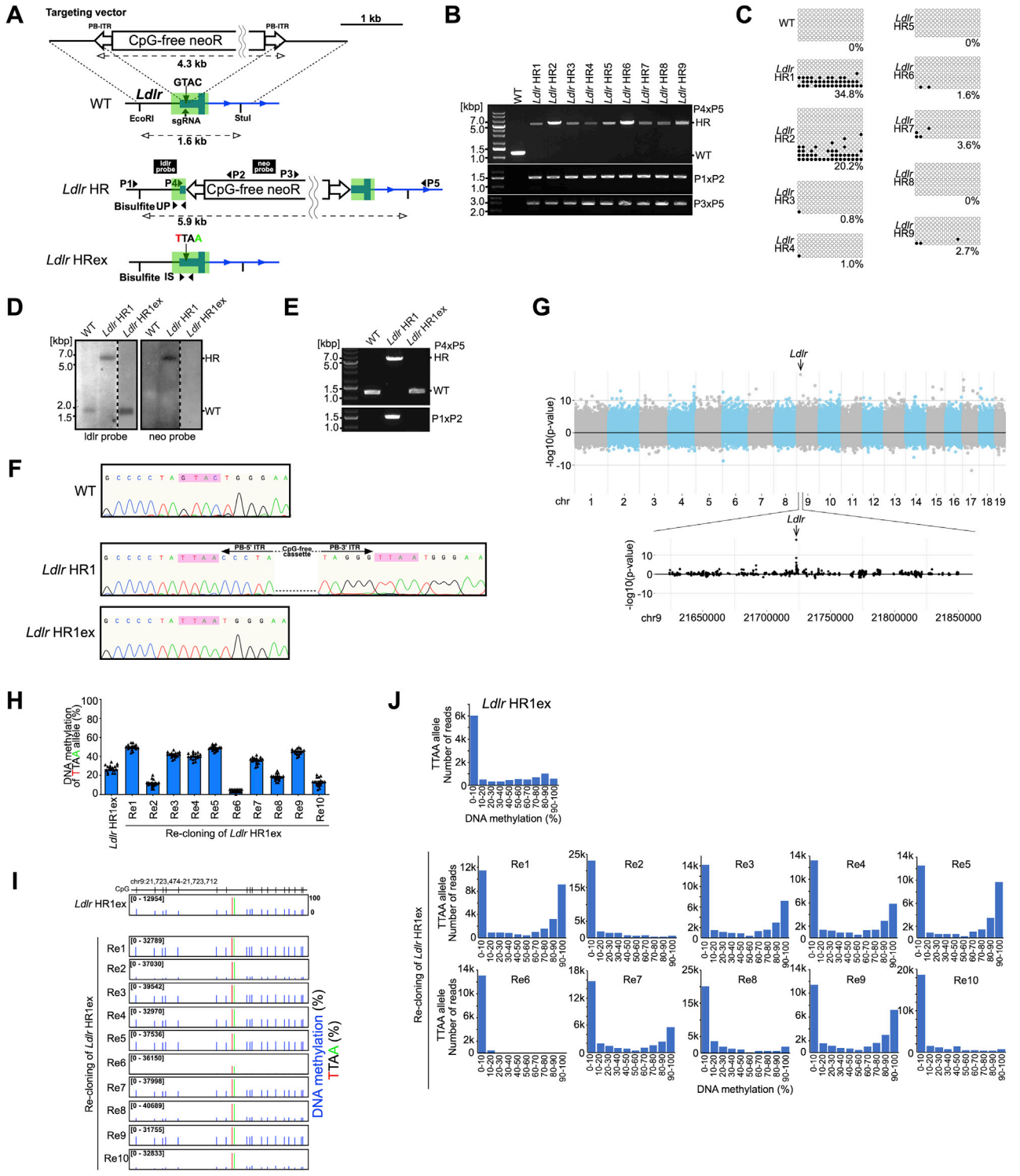

Figure S2. *Ldlr* CGI methylation established by integration of CpG-free DNA in mESCs, related to Figure 1

(A) A schematic of integration of CpG-free DNA into *Ldlr* CGI through HR and removal of the cassette in mESCs. Filled arrowheads represent PCR primers. Black bars with probe inside represent probes for southern blot analysis. Green boxes represent CpG island of *Ldlr*.

(B) Genotyping of the *Ldlr* HR clones. The primers for PCR are shown in (A).

(C) Bisulfite sequencing analysis of upstream region of CpG-free DNA integration site within *Ldlr* CGI. The primers for PCR are shown in (A).

(legend continued on next page)

(D) Southern blot analysis of WT, *Ldlr* HR1, and *Ldlr* HR1ex. Genomic DNA was digested with EcoRI and StuI. Targeted regions were detected by ldlr probe (left) or *neo* probe (right). The probes are shown in (A).
(E) Genotyping of the *Ldlr* HR1 and HR1ex clones. The primers for PCR are shown in (A).
(F) Genomic DNA sequence of HR site in WT, *Ldlr* HR1, and *Ldlr* HR1ex. Pink boxes represent the WT sequence, GTAC, and the sequence after targeting, TTAA.
(G) A Manhattan plot of differentially methylated regions between WT mESC and *Ldlr* HR1ex from WGBS. See also Table S2.
(H–J) Bisulfite sequencing analysis showing DNA methylation status of *Ldlr* CGI in *Ldlr* HR1ex clone and re-clones. While in the original *Ldlr* HR1ex clone, 20% of TTAA alleles were highly methylated and half of them were almost unmethylated, nine of ten re-clones exhibited a similar DNA methylation distribution with that of the original clone. (H) Data represent mean ± SEM of methylation status of the 18 CpG sites in the CGIs. (I) Each bar represents the methylation status of a single CpG site or percentage of TTAA. Number of mapped reads is shown in the columns. (J) Distribution of reads by DNA methylation status.

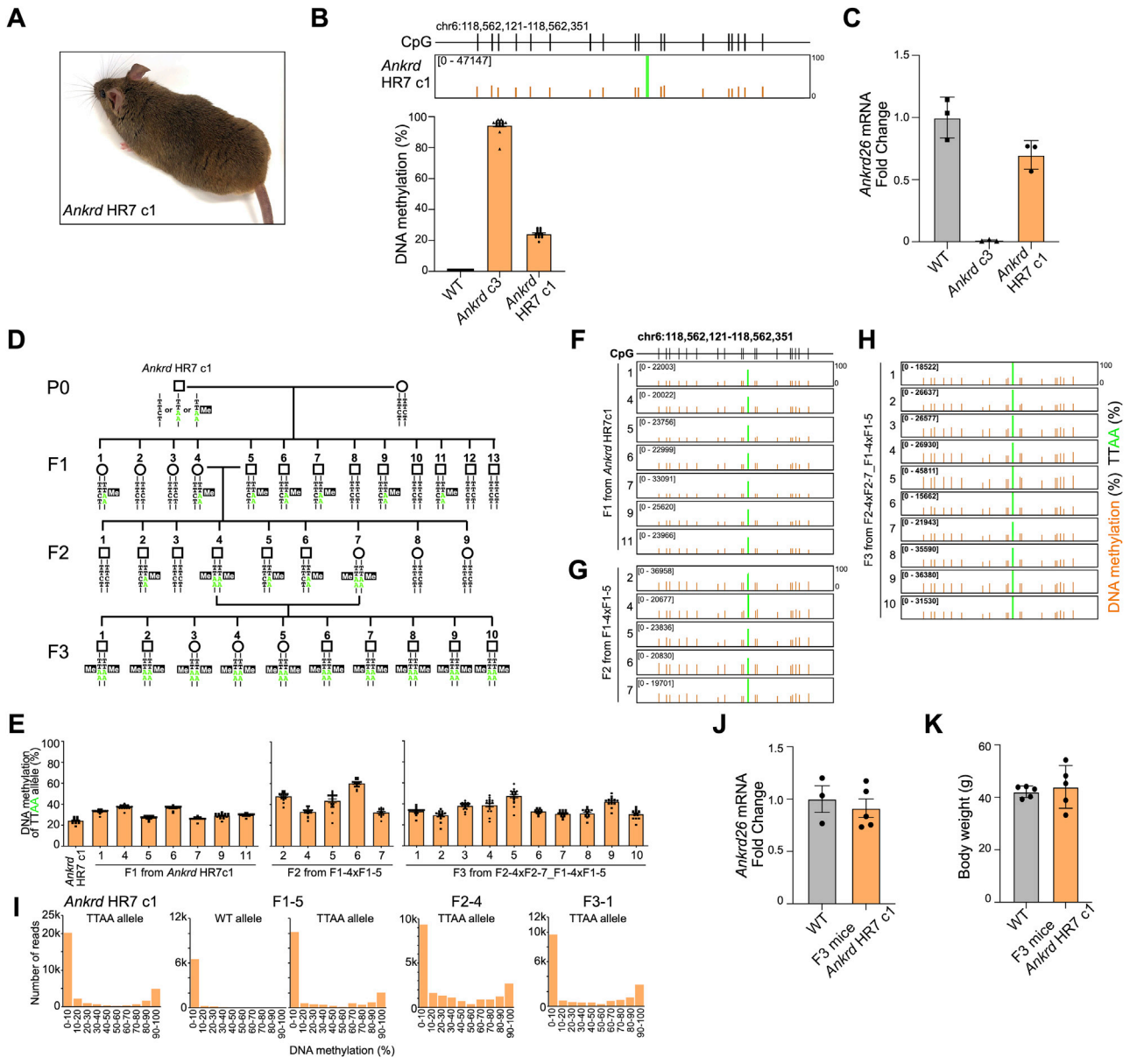

Figure S3. Transgenerational inheritance of low methylation at *Ankrd26* CGI in *Ankrd* HR7 c1 mouse line, related to Figures 2 and 3

(A) *Ankrd* HR7c1 mouse at 6 months of ages.

(B and E–I) Bisulfite sequencing analysis showing DNA methylation status of *Ankrd26* CGI. (B upper and F–H) Each bar represents methylation status of a single CpG site or percentage of TTAA allele. (B lower and E) Data represent mean ± SEM of methylation status of the 18 CpG sites in *Ankrd26* CGI of mapped reads (B lower) and of TTAA allele (E). (I) Distribution of reads by DNA methylation status.

(C and J) Quantitative RT-PCR analysis of *Ankrd26* mRNA expression normalized to *Gapdh* mRNA. (C) Error bars indicate ±SEM of three independent experiments. (J) WT; n = 3, F3 mice of *Anked* HR7 mice; n = 5.

(D) A pedigree of offspring from *Ankrd* HR7c1.

(K) Body weight of male F3 *Anked* HR7 mice (n = 5) and male ICR WT mice (n = 5) at 40 weeks of ages. Data are expressed as mean ± SEM.

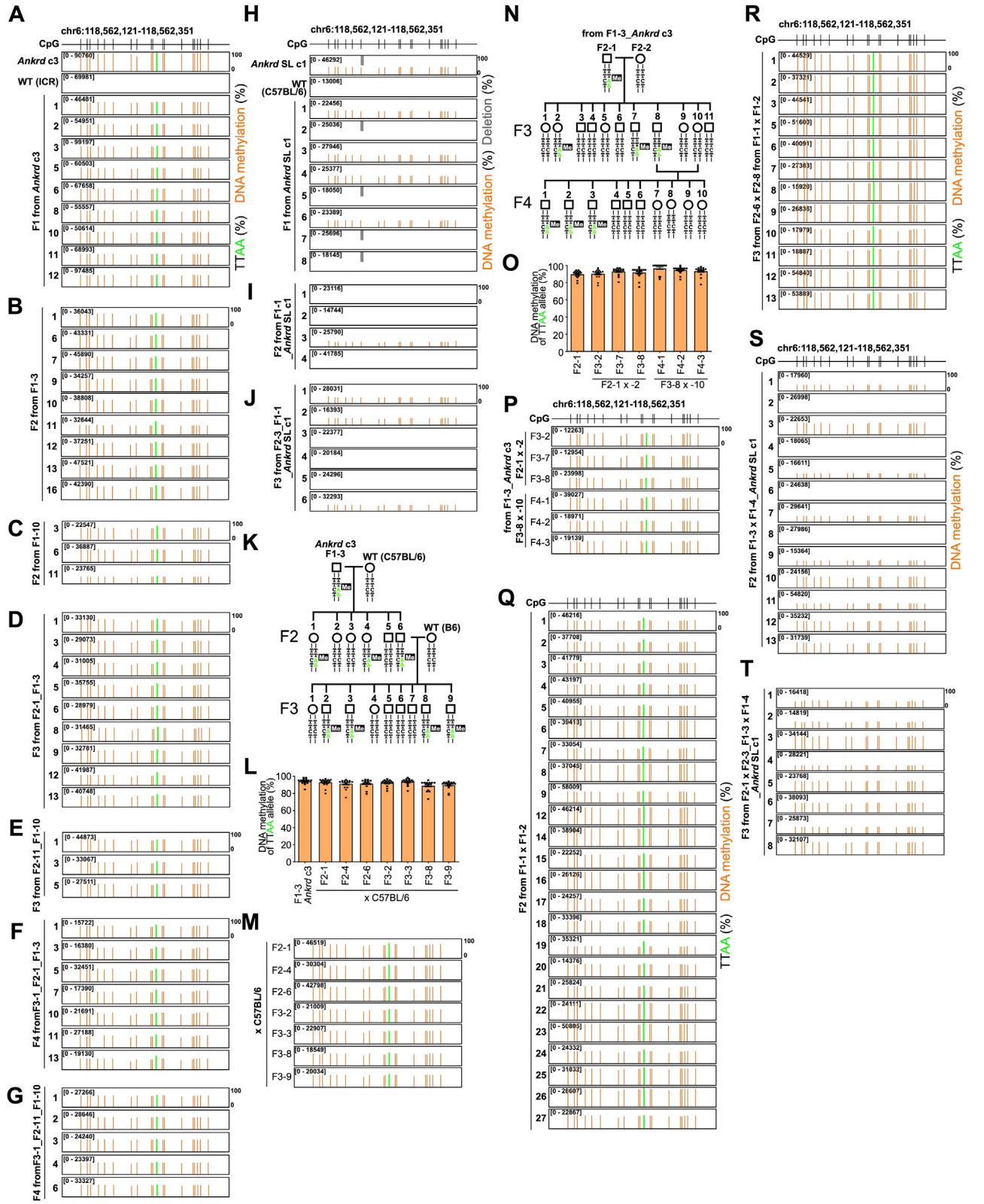

(legend on next page)

Figure S4. Transgenerational inheritance of DNA methylation at *Ankrd26* CGI in *Ankrd* c3 mouse line and *Ankrd* SL c1 mouse line, related to Figures 3 and 5

(A–J, L, M, and O–T) Bisulfite sequencing analysis showing DNA methylation status of *Ankrd26* CGI. (A–J, M, and P–T) Each bar represents methylation status of a single CpG site or percentage of TTAA allele. Number of mapped reads is shown in the columns. (L and O) Data represent mean ± SEM of methylation status of the 18 CpG sites in *Ankrd26* CGI of TTAA allele.

(K and N) Pedigrees of offspring from *Ankrd* c3 line.

(K–P) Toward accelerating the studies of transgenerational epigenetic inheritance, we used the outbred mouse line ICR (which have superior characteristics, including excellent fecundity and rapid growth), for outcrosses with the chimeras, *Ankrd* c3 and *Ankrd* HR7 and their offspring. Though it is assumed that outbred mice may have trait variability, it should be noted that DNA methylation of *Ankrd26* CGI and *Ldlr* CGI was definitely never observed in WT mice of the outbred ICR line and other inbred mouse lines. To confirm whether mouse background affects the transgenerational inheritance of *Ankrd26* CGI methylation, we crossed the F1-3 mouse from the *Ankrd* c3 to a C57BL/6 female. Similar to crossing to ICR mice, the methylation of the *Ankrd26* CGI is stably transmitted across multiple generations (K–M). To further examine whether mouse background has any effect, we carried out a sibling mating between the F2-1 offspring with a methylated TTAA allele and the F2-2, not inherited TTAA allele, from the F1-3. Similar to a cross between the F2-1 and ICR mouse, the offspring resulting from the sibling mating also inherited DNA methylation of the *Ankrd26* CGI (N–P).

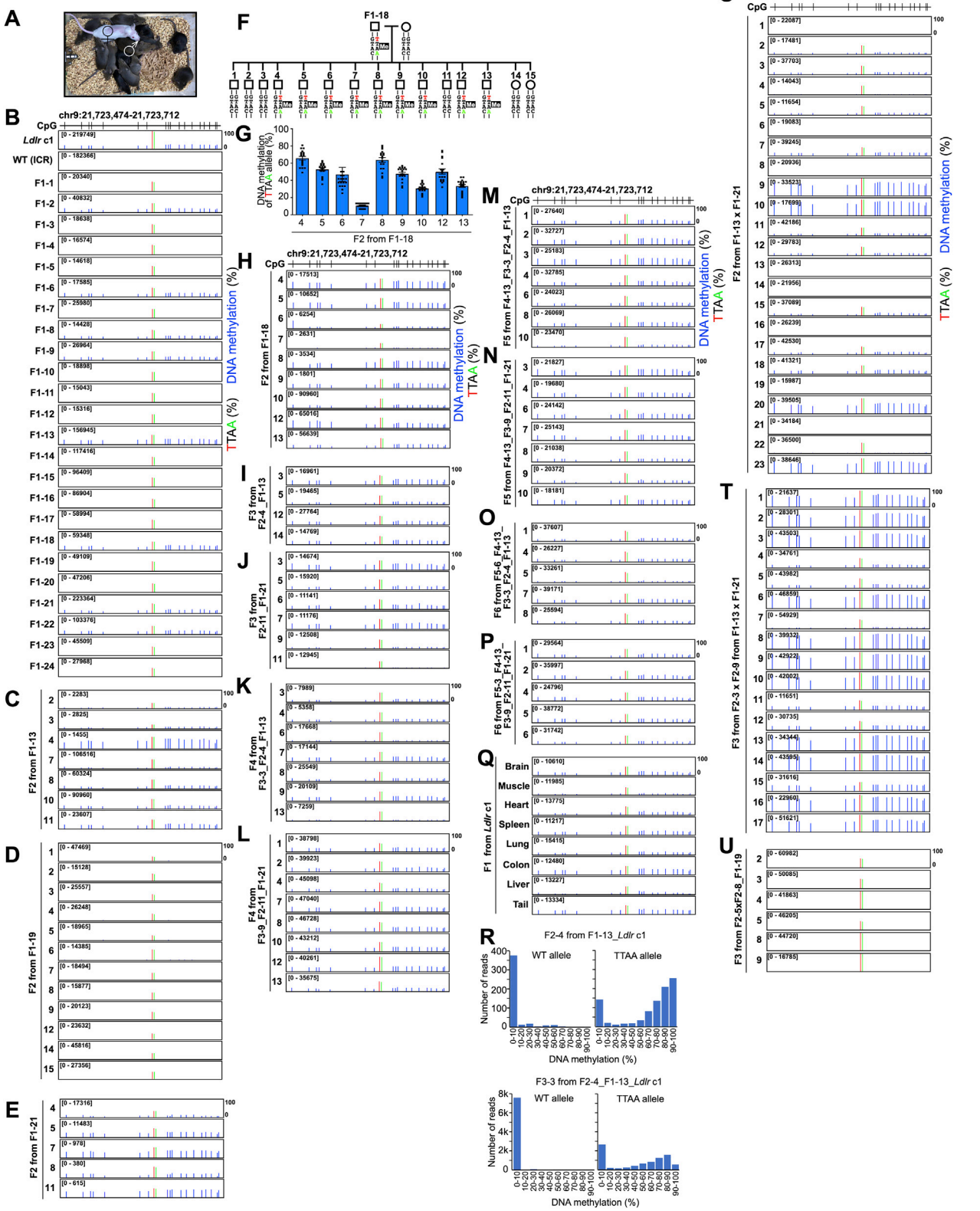

(legend on next page)

Figure S5. Transgenerational inheritance of DNA methylation at *Ldlr* CGI in *Ldlr* c1 mouse line, related to Figures 4 and 6

(A) F1 offspring from *Ldlr* c1. ♂ and ♀ represent the sire *Ldlr* c1 and the dam WT ICR, respectively.

(B–E, G–Q, and S–U) Bisulfite sequencing analysis showing DNA methylation status of *Ldlr*. (B–E, H–Q, and S–U) Each bar represents methylation status of a single CpG site or percentage of TTAA allele. Number of mapped reads is shown in the columns. (G) Data represent mean ± SEM of methylation status of the 18 CpG sites in the CGIs of the TTAA alleles.

(F) A pedigree of offspring from F1-18.

(R) Distribution of reads by DNA methylation status. The reads of bisulfite sequencing were sorted into two groups (WT allele or TTAA allele) and then were distributed by percentage of DNA methylation of each read.

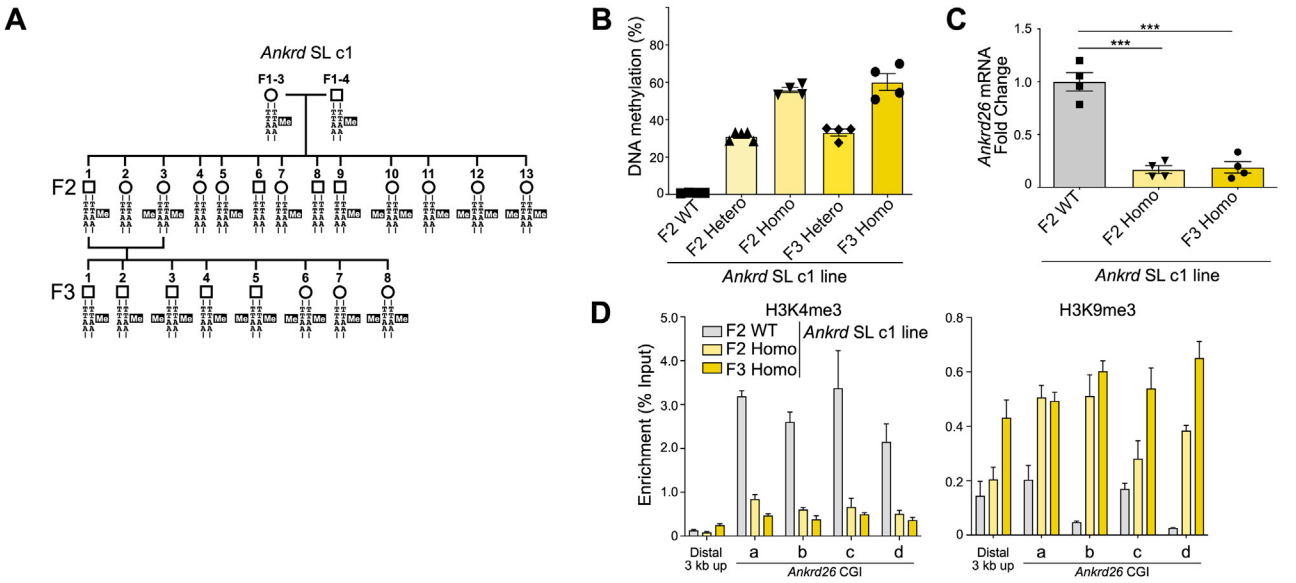

Figure S6. The gene silencing and a closed chromatin status on the *Ankrd26* CGI were transmitted to offspring in the *Ankrd* SL c1 line, related to Figure 5

(A) A pedigree of offspring from *Ankrd* SL c1.

(B) Bisulfite sequencing analysis. Data are expressed as mean ± SEM of DNA methylation status of *Ankrd26* CGI in F2 and F3 offspring from *Ankrd* SL c1. See also Figure S4.

(C) Quantitative RT-PCR analysis of *Ankrd26* mRNA expression. Error bars indicate ±SEM. Versus WT; ***$p < 0.0001$ by unpaired Student's t test.

(D) ChIP-qPCR analysis of H3K4me3 and H3K9me3 across *Ankrd26* CGI locus in the F2 (WT; n = 3, homo; n = 3) and F3 offspring (homo; n = 3) from *Ankrd* SL c1. Error bars indicate ±SD from triplicate experiments.

(A–D) To confirm whether gene repression and chromatin status can be transmitted in the *Ankrd* SL c1 line, we crossed a heterozygous methylated F1 female (F1-3) with a heterozygous methylated F1 male (F1-4). Among the thirteen F2 offspring, 4 mice exhibited almost no methylation, 5 mice exhibited around 30% methylation and 4 mice exhibited around 60% methylation at the *Ankrd26* CGI. Given the results showing that induced methylation of CGIs is stably transmitted to offspring (Figures 3, 4, and 5), it could be assumed that the around 30% of methylated mice heterogeneously inherited a methylated allele and that around 60% of the methylated mice are homozygous methylated mice, though we can not definitively conclude it is due to an absence of allele specific SNVs. In the homozygous F2 and F3 mice, expression of *Ankrd26* mRNA was repressed and the levels of the active mark H3K4me3 on the *Ankrd26* CGI were diminished, whereas the levels of the repressive mark H3K9me3 were highly increased.

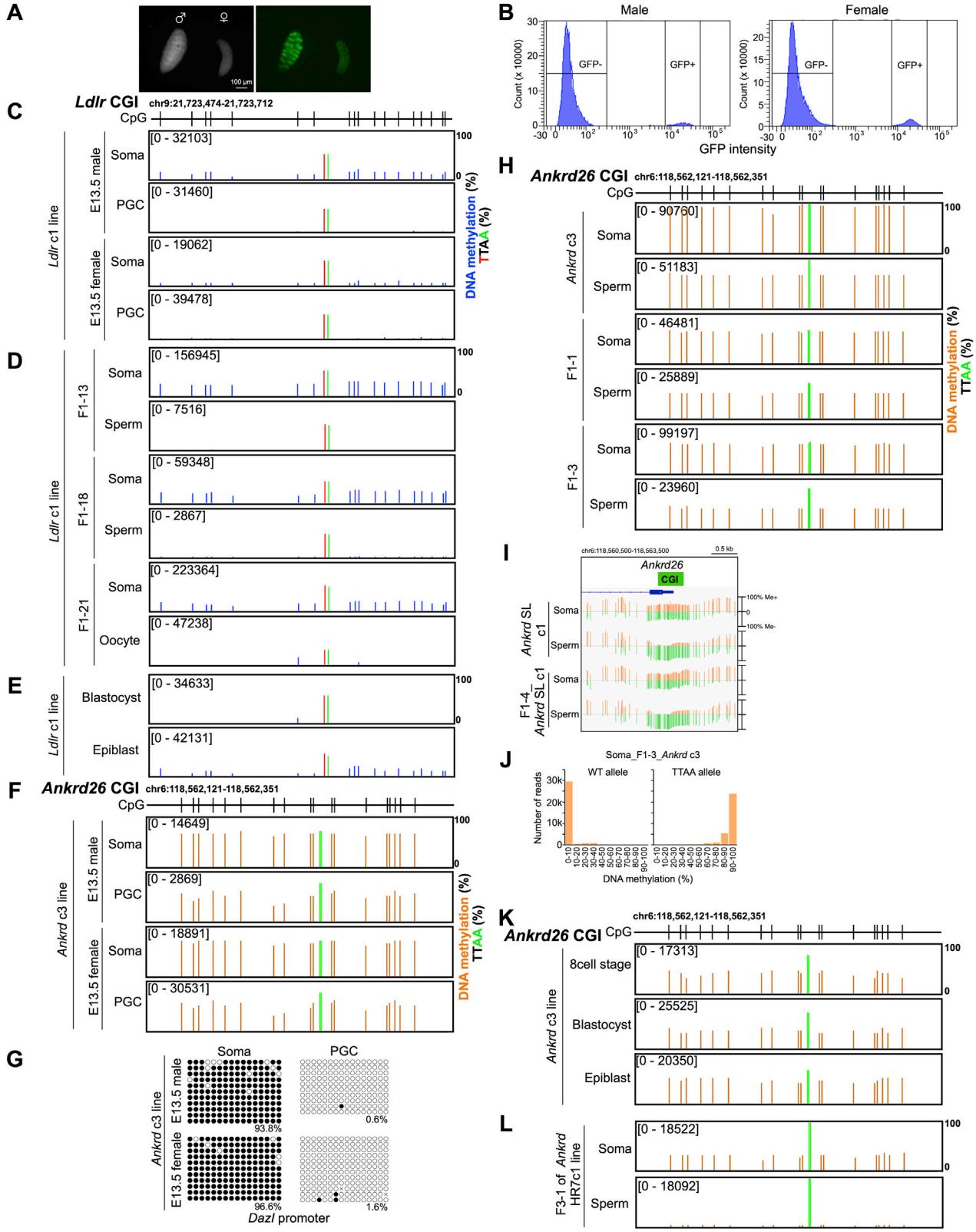

(legend on next page)

Figure S7. DNA methylation status of *Ldlr* CGI and *Ankrd26* CGI in the germ cells and embryos, related to Figure 7

(A) PGCs expressing GFP in E13.5 male and female gonads.

(B) Isolation of PGCs from E13.5 gonads by FACS sorting depending on GFP signal.

(C–H, K, and L) Bisulfite sequencing analysis showing DNA methylation status of *Ldlr* CGI (C–E), *Ankrd26* CGI (F, H, K, and L), and *Dazl* promoter (G). Each bar represents methylation status of a single CpG site or percentage of TTAA allele. Number of mapped reads is shown in the columns.

(I) Target enrichment-genome bisulfite sequencing analysis showing methylation status of a region (chr6:118560500-118563500) in the targeted enrichment locus. Each vertical bar represents methylation status at a single CpG. Me+ and Me− represent methylated and unmethylated status, respectively.

(J) Distribution of reads by DNA methylation status. The reads of bisulfite sequencing were sorted into two groups (WT allele or TTAA allele) and then were distributed by percentage of DNA methylation of each read.